Table 2 Prognostic impacts of clinicopathological variables computed by Cox's univariate and multivariate analyses in patients with primary breast cancer

		Univariate			Multivariate		
		Hazard ratio	(95% CI)	P-value	Hazard ratio	(95%CI)	P-value
Disease free survival							
Nucleostemin	Negative	1		0.023	1		0.036
	Positive	2.06	(1.11-3.84)		2.13	(1.05-4.33)	
Hormone-receptor	Positive	1		0.045	1		0.46
	Negative	1.73	(1.01-2.95)		0.78	(0.39-1.52)	
HER2	Negative	1		0.0005	1		0.17
	Positive	2.91	(1.59-5.34)		1.65	(0.80-3.41)	
Nuclear grade	1, 2	1		<0.0001	1		0.0008
	3	3.30	(1.94-5.64)		2.97	(1.57-5.61)	
Tumor size	≦5.0 cm	1		<0.0001	1		0.0007
	>5.0 cm	6.89	(3.97-11.9)		2.99	(1.59-5.66)	
Nodal status	Negative	1		<0.0001	1		0.0038
	Positive	4.51	(2.45-8.31)		2.73	(1.38-5.38)	
Distant metastasis	Negative	1		<0.0001	1		<0.0001
	Positive	71.6	(26.1-196.5)		62.3	(15.5-251.1)	

Abbreviation: 95% CI 95% confidence interval.

indicator in several human cancer types [24,26-30]. Based on these observations, our results show that high NS expression is a powerful indicator of poor outcome, consistent with the idea that NS may be a breast cancer stem cell marker.

The limitations of the present study included the retrospective analyses and the heterogeneity of adjuvant treatments. Therefore, one should pay careful attention when interpreting these results. Further studies using a uniformly treated patient cohort are required to clarify the role of NS in breast cancer stem cells.

We found that the patient group with tumors coexpressing NS and p53 had shorter DFS times than the patient group with tumors negative for either NS or p53. GTP binding modulates the movement of NS from the nucleoli to the nucleoplasm; NS then binds p53 at its N-terminal basic domain, which results in the suppression of p53 function [6,7]. Because prolongation of the half-life of most of the mutated p53 protein induces its nuclear accumulation, it is generally believed that the p53 pathway does not fully function in tumors with high p53 nuclear immunoreactivity [31-33]. This evidence leads to the assumption that p53 function would be profoundly suppressed in tumors coexpressing NS and p53. Our results show the validity of this concept and that functional crosstalk between NS and p53 may also occur *in vivo*.

Currently, we cannot explain the correlation between NS expression and p53 expression. Although several studies have shown that NS modulates the expression of wild-type p53 [34,35], the role of NS in breast cancers with mutant p53 has not yet been evaluated. Further research is needed to elucidate the correlation.

We found that the NS expression status was positively correlated with both ER and HER2 status and also found a significant prognostic implication of NS expression for patients with luminal-type tumors and those with HER2-type tumors, except for those with triple-negative tumors. NS was first identified as a gene upregulated in MCF-7 cells upon 17β-estradiol treatment [36]; therefore, our inclusion of subgroup analysis among patients with luminal-type tumors was reasonable. To our knowledge, this is the first report to demonstrate the possible association between NS and HER2. Zhang G et al. showed that NS is required for the expression of EGF and EGFR in an esophageal squamous carcinoma cell line [13]. Presumably, NS is required for the expression of HER2 in a manner similar to that for EGFR. We found no survival impact of the NS expression status among patients with triple-negative tumors, who show higher rates of mutated p53 than patients with luminal-type or HER2-type tumors [37]. NS can function in the presence of wide-type p53 [7]; therefore, the expression status of NS may have survival impact only for the luminal-type and HER2-type tumors.

Conclusions

In summary, our results indicate that the expression status of NS, abundant in stem cells, is a prognostic indicator in breast cancer patients, especially for those with

luminal-type or HER2-type tumors, and that the co-expression of NS and p53 correlates with poorer prognostic outcomes. Examination of NS expression may be useful for the stratification and management of breast cancer patients in future daily practice.

Competing interests
The authors declare no conflicts of interest.

Authors' contributions
TK and HT conceived of the study, performed experiments, analyzed data and wrote the manuscript. TM, TY, and JY provided samples, collected clinical and pathological data. KM, KT, YF, and ST participated in designing the study and revising the manuscript. HT participated in the overall design and study coordination and finalized the draft of the manuscript. All authors read and approved the final manuscript.

Acknowledgments
This work was supported in part by the Foundation for Promotion of Defense Medicine and by the Cancer Research and Development Fund from the National Cancer Center, Japan.

Author details
[1]*Department of Basic Pathology, National Defense Medical College, 3-2 Namiki, Tokorozawa, Saitama 359-8513, Japan.* [2]Department of Medical Oncology, Cancer Institute Hospital, 3-8-31 Ariake, Koto-ku, Tokyo 135-8550, Japan. [3]Division of Cancer Stem Cell, National Cancer Center Research Institute, Tsukiji, Chuo-ku, Tokyo 104-0045, Japan. [4]Department of Breast Oncology and Medical Oncology, National Cancer Center Hospital, 5-1-1 Tsukiji, Chuo-ku, Tokyo 104-0045, Japan. [5]Department of Surgery, National Defense Medical College, 3-2 Namiki, Tokorozawa, Saitama 359-8513, Japan. [6]Department of Pathology and Clinical Laboratories, National Cancer Center Hospital, 5-1-1 Tsukiji, Chuo-ku, Tokyo 104-0045, Japan.

Received: 19 October 2013 Accepted: 11 March 2014
Published: 21 March 2014

References
1. O'Shaughnessy J: **Extending survival with chemotherapy in metastatic breast cancer.** *Oncologist* 2005, **10**(Suppl 3):20–29.
2. Pagani O, Senkus E, Wood W, Colleoni M, Cufer T, Kyriakides S, Costa A, Winer EP, Cardoso F: **International guidelines for management of metastatic breast cancer: can metastatic breast cancer be cured?** *J Natl Cancer Inst* 2010, **102**(7):456–463.
3. Clarke MF, Fuller M: **Stem cells and cancer: two faces of eve.** *Cell* 2006, **124**(6):1111–1115.
4. Reya T, Morrison SJ, Clarke MF, Weissman IL: **Stem cells, cancer, and cancer stem cells.** *Nature* 2001, **414**(6859):105–111.
5. Dean M, Fojo T, Bates S: **Tumour stem cells and drug resistance.** *Nat Rev Cancer* 2005, **5**(4):275–284.
6. Tsai RY, McKay RD: **A nucleolar mechanism controlling cell proliferation in stem cells and cancer cells.** *Genes Dev* 2002, **16**(23):2991–3003.
7. Bernardi R, Pandolfi PP: **The nucleolus: at the stem of immortality.** *Nat Med* 2003, **9**(1):24–25.
8. Ye F, Zhou C, Cheng Q, Shen J, Chen H: **Stem-cell-abundant proteins Nanog, Nucleostemin and Musashi1 are highly expressed in malignant cervical epithelial cells.** *BMC Cancer* 2008, **8**:108.
9. Fan Y, Liu Z, Zhao S, Lou F, Nilsson S, Ekman P, Xu D, Fang X: **Nucleostemin mRNA is expressed in both normal and malignant renal tissues.** *Br J Cancer* 2006, **94**(11):1658–1662.
10. Liu RL, Zhang ZH, Zhao WM, Wang M, Qi SY, Li J, Zhang Y, Li SZ, Xu Y: **Expression of nucleostemin in prostate cancer and its effect on the proliferation of PC-3 cells.** *Chin Med J (Engl)* 2008, **121**(4):299–304.
11. Cada Z, Boucek J, Dvorankova B, Chovanec M, Plzak J, Kodets R, Betka J, Pinot GL, Gabius HJ, Smetana K Jr: **Nucleostemin expression in squamous cell carcinoma of the head and neck.** *Anticancer Res* 2007, **27**(5A):3279–3284.
12. Malakootian M, Mowla SJ, Saberi H, Asadi MH, Atlasi Y, Shafaroudi AM: **Differential expression of nucleostemin, a stem cell marker, and its variants in different types of brain tumors.** *Mol Carcinog* 2010, **49**(9):818–825.
13. Zhang G, Zhang Q, Yin L, Li S, Cheng K, Zhang Y, Xu H, Wu W: **Expression of nucleostemin, epidermal growth factor and epidermal growth factor receptor in human esophageal squamous cell carcinoma tissues.** *J Cancer Res Clin Oncol* 2010, **136**(4):587–594.
14. Tamase A, Muraguchi T, Naka K, Tanaka S, Kinoshita M, Hoshii T, Ohmura M, Shugo H, Ooshio T, Nakada M, Sawamoto K, Onodera M, Matsumoto K, Oshima M, Asano M, Saya H, Okano H, Suda T, Hamada J, Hirao A: **Identification of tumor-initiating cells in a highly aggressive brain tumor using promoter activity of nucleostemin.** *Proc Natl Acad Sci U S A* 2009, **106**(40):17163–17168.
15. Okamoto N, Yasukawa M, Nguyen C, Kasim V, Maida Y, Possemato R, Shibata T, Ligon KL, Fukami K, Hahn WC, Masutomi K: **Maintenance of tumor initiating cells of defined genetic composition by nucleostemin.** *Proc Natl Acad Sci U S A* 2011, **108**(51):20388–20393.
16. Kobayashi T, Tsuda H, Moriya T, Yamasaki T, Kikuchi R, Ueda S, Omata J, Yamamoto J, Matsubara O: **Expression pattern of stromal cell-derived factor-1 chemokine in invasive breast cancer is correlated with estrogen receptor status and patient prognosis.** *Breast Cancer Res Treat* 2010, **123**(3):733–745.
17. Nakajima TE, Yoshida H, Okamoto N, Nagashima K, Taniguchi H, Yamada Y, Shimoda T, Masutomi K: **Nucleostemin and TWIST as predictive markers for recurrence after neoadjuvant chemotherapy for esophageal carcinoma.** *Cancer Sci* 2012, **103**(2):233–238.
18. Wolff AC, Hammond ME, Schwartz JN, Hagerty KL, Allred DC, Cote RJ, Dowsett M, Fitzgibbons PL, Hanna WM, Langer A, McShane LM, Paik S, Pegram MD, Perez EA, Press MF, Rhodes A, Sturgeon C, Taube SE, Tubbs R, Vance GH, van de Vijver M, Wheeler TM, Hayes DF: **American Society of Clinical Oncology/College of American Pathologists guideline recommendations for human epidermal growth factor receptor 2 testing in breast cancer.** *J Clin Oncol* 2007, **25**(1):118–145.
19. Yoshida R, Fujimoto T, Kudoh S, Nagata M, Nakayama H, Shinohara M, Ito T: **Nucleostemin affects the proliferation but not differentiation of oral squamous cell carcinoma cells.** *Cancer Sci* 2011, **102**(7):1418–1423.
20. Al-Hajj M, Wicha MS, Benito-Hernandez A, Morrison SJ, Clarke MF: **Prospective identification of tumorigenic breast cancer cells.** *Proc Natl Acad Sci U S A* 2003, **100**(7):3983–3988.
21. O'Brien CA, Pollett A, Gallinger S, Dick JE: **A human colon cancer cell capable of initiating tumour growth in immunodeficient mice.** *Nature* 2007, **445**(7123):106–110.
22. Ricci-Vitiani L, Lombardi DG, Pilozzi E, Biffoni M, Todaro M, Peschle C, De Maria R: **Identification and expansion of human colon-cancer-initiating cells.** *Nature* 2007, **445**(7123):111–115.
23. Singh SK, Hawkins C, Clarke ID, Squire JA, Bayani J, Hide T, Henkelman RM, Cusimano MD, Dirks PB: **Identification of human brain tumour initiating cells.** *Nature* 2004, **432**(7015):396–401.
24. Ginestier C, Hur MH, Charafe-Jauffret E, Monville F, Dutcher J, Brown M, Jacquemier J, Viens P, Kleer CG, Liu S, Schott A, Hayes D, Birnbaum D, Wicha MS, Dontu G: **ALDH1 is a marker of normal and malignant human mammary stem cells and a predictor of poor clinical outcome.** *Cell Stem Cell* 2007, **1**(5):555–567.
25. Hermann PC, Huber SL, Herrler T, Aicher A, Ellwart JW, Guba M, Bruns CJ, Heeschen C: **Distinct populations of cancer stem cells determine tumor growth and metastatic activity in human pancreatic cancer.** *Cell Stem Cell* 2007, **1**(3):313–323.
26. Joensuu H, Klemi PJ, Toikkanen S, Jalkanen S: **Glycoprotein CD44 expression and its association with survival in breast cancer.** *Am J Pathol* 1993, **143**(3):867–874.
27. Tempfer C, Losch A, Heinzl H, Hausler G, Hanzal E, Kolbl H, Breitenecker G, Kainz C: **Prognostic value of immunohistochemically detected CD44 isoforms CD44v5, CD44v6 and CD44v7-8 in human breast cancer.** *Eur J Cancer* 1996, **32A**(11):2023–2025.
28. Horst D, Kriegl L, Engel J, Kirchner T, Jung A: **CD133 expression is an independent prognostic marker for low survival in colorectal cancer.** *Br J Cancer* 2008, **99**(8):1285–1289.
29. Maeda S, Shinchi H, Kurahara H, Mataki Y, Maemura K, Sato M, Natsugoe S, Aikou T, Takao S: **CD133 expression is correlated with lymph node metastasis and vascular endothelial growth factor-C expression in pancreatic cancer.** *Br J Cancer* 2008, **98**(8):1389–1397.
30. Marechal R, Demetter P, Nagy N, Berton A, Decaestecker C, Polus M, Closset J, Deviere J, Salmon I, Van Laethem JL: **High expression of CXCR4 may predict poor survival in resected pancreatic adenocarcinoma.** *Br J Cancer* 2009, **100**(9):1444–1451.

31. Davidoff AM, Herndon JE 2nd, Glover NS, Kerns BJ, Pence JC, Iglehart JD, Marks JR: **Relation between p53 overexpression and established prognostic factors in breast cancer.** *Surgery* 1991, **110**(2):259–264.
32. Bartek J, Bartkova J, Lukas J, Staskova Z, Vojtesek B, Lane DP: **Immunohistochemical analysis of the p53 oncoprotein on paraffin sections using a series of novel monoclonal antibodies.** *J Pathol* 1993, **169**(1):27–34.
33. Soussi T, Legros Y, Lubin R, Ory K, Schlichtholz B: **Multifactorial analysis of p53 alteration in human cancer: a review.** *Int J Cancer* 1994, **57**(1):1–9.
34. Ma H, Pederson T: **Depletion of the nucleolar protein nucleostemin causes G1 cell cycle arrest via the p53 pathway.** *Mol Biol Cell* 2007, **18**(7):2630–2635.
35. Dai MS, Sun XX, Lu H: **Aberrant expression of nucleostemin activates p53 and induces cell cycle arrest via inhibition of MDM2.** *Mol Cell Biol* 2008, **28**(13):4365–4376.
36. Charpentier AH, Bednarek AK, Daniel RL, Hawkins KA, Laflin KJ, Gaddis S, MacLeod MC, Aldaz CM: **Effects of estrogen on global gene expression: identification of novel targets of estrogen action.** *Cancer Res* 2000, **60**(21):5977–5983.
37. Sorlie T, Perou CM, Tibshirani R, Aas T, Geisler S, Johnsen H, Hastie T, Eisen MB, van de Rijn M, Jeffrey SS, Thorsen T, Quist H, Matese JC, Brown PO, Botstein D, Eystein Lonning P, Borresen-Dale AL: **Gene expression patterns of breast carcinomas distinguish tumor subclasses with clinical implications.** *Proc Natl Acad Sci U S A* 2001, **98**(19):10869–10874.

doi:10.1186/1471-2407-14-215
Cite this article as: Kobayashi *et al.*: Nucleostemin expression in invasive breast cancer. *BMC Cancer* 2014 **14**:215.

CANCER

Exosomes from bone marrow mesenchymal stem cells contain a microRNA that promotes dormancy in metastatic breast cancer cells

Makiko Ono,[1] Nobuyoshi Kosaka,[1] Naoomi Tominaga,[1] Yusuke Yoshioka,[1] Fumitaka Takeshita,[1] Ryou-u Takahashi,[1] Masayuki Yoshida,[2] Hitoshi Tsuda,[3] Kenji Tamura,[4] Takahiro Ochiya[1]*

Breast cancer patients often develop metastatic disease years after resection of the primary tumor. The patients are asymptomatic because the disseminated cells appear to become dormant and are undetectable. Because the proliferation of these cells is slowed, dormant cells are often unresponsive to traditional chemotherapies that exploit the rapid cell cycling of most cancer cells. We generated a bone marrow–metastatic human breast cancer cell line (BM2) by tracking and isolating fluorescent-labeled MDA-MB-231 cells that disseminated to the bone marrow in mice. Coculturing BM2 cells with bone marrow mesenchymal stem cells (BM-MSCs) isolated from human donors revealed that BM-MSCs suppressed the proliferation of BM2 cells, decreased the abundance of stem cell–like surface markers, inhibited their invasion through Matrigel Transwells, and decreased their sensitivity to docetaxel, a common chemotherapy agent. Acquisition of these dormant phenotypes in BM2 cells was also observed by culturing the cells in BM-MSC–conditioned medium or with exosomes isolated from BM-MSC cultures, which were taken up by BM2 cells. Among various microRNAs (miRNAs) increased in BM-MSC–derived exosomes compared with those from adult fibroblasts, overexpression of miR-23b in BM2 cells induced dormant phenotypes through the suppression of a target gene, *MARCKS*, which encodes a protein that promotes cell cycling and motility. Metastatic breast cancer cells in patient bone marrow had increased *miR-23b* and decreased *MARCKS* expression. Together, these findings suggest that exosomal transfer of miRNAs from the bone marrow may promote breast cancer cell dormancy in a metastatic niche.

INTRODUCTION

Breast cancer is the most common cancer; about 70,000 cases were newly diagnosed in 2010, with more than 12,000 deaths reported in 2012 in Japan (*1*). Although breast cancer mortality in Western countries is decreasing because of early detection and effective systemic adjuvant therapy, breast cancer recurrence often occurs, typically within 5 years but even up to 10 to 20 years after surgery (*2*). Because recurrence is often more aggressive and untreatable, it is important to identify the mechanisms that enable therapeutic subversion and regrowth. This phenomenon indicates that breast cancer cells survive for a long time somewhere in the body in a state of cancer dormancy, in which cells cease dividing but survive in a quiescent state while waiting for appropriate environmental conditions to begin proliferation again. Clinical reports show that disseminated breast cancer cells can be detected in the bone marrow (BM) at early stages of breast cancer and is a strong prognostic factor (*3*). Bone marrow is a common homing tissue for disseminated tumor cells, many of which have surface abundance of CD44 but not CD24 ($CD44^+$ and $CD24^-$), a characteristic common to breast cancer stem cells (CSCs) (*4*). It is thought that micrometastases form in the bone marrow and then recirculate to invade other, distant organs (*5*).

By contrast, hematopoietic stem cells, which have the properties of self-renewal and pluripotency, are thought to be regulated by signals derived from the bone marrow microenvironment, called the bone marrow niche.

Hematopoietic stem cell niches are composed of several cell types, including endothelial cells (*6*), osteoblasts (*7–9*), chemokine ligand 12–abundant reticular cells (*10*), nonmyelinating Schwann cells (*11*), and bone marrow mesenchymal stem cells (BM-MSCs) (*12*). These cells appear to control the self-renewal, differentiation, hibernation, and mobilization of hematopoietic stem cells. It is thought that CSCs may form a niche similar to that of hematopoietic stem cells; indeed, some reports have demonstrated the existence of niche-regulating CSCs (*13*, *14*). Furthermore, because BM-MSCs have been found to be associated with breast cancer metastases (*15*), we hypothesized that breast CSCs, similar to hematopoietic stem cells, have a niche composed of BM-MSCs.

Exosomes, which are small intraluminal vesicles of multivesicular bodies released upon exocytic fusion with plasma membranes, are secreted from numerous types of cells and function in intercellular communication by transporting intracellular contents, such as protein, mRNA, and microRNAs (miRNAs) (*16*, *17*). Exosomes secreted by cancer cells may play an important role in cancer progression by promoting angiogenesis (*18*), neutrophil infiltration (*19*), and the education of bone marrow–derived cells (*20*). In turn, exosomes secreted by stromal cells in the tumor microenvironment may contribute to cancer progression through the transmission of their cargo to cancer cells (*21*, *22*). Therefore, we hypothesized that exosomes secreted by BM-MSCs could influence the dormant state of metastatic breast CSCs and investigated the molecular cargo that enabled this switch.

[1]Division of Molecular and Cellular Medicine, National Cancer Center Research Institute, Tokyo 104-0045, Japan. [2]Department of Pathology and Clinical Laboratories, National Cancer Center Hospital, Tokyo 104-0045, Japan. [3]Department of Pathology, National Defense Medical College, Saitama 359-0042, Japan. [4]Breast and Medical Oncology Division, National Cancer Center Hospital, Tokyo 104-0045, Japan.
*Corresponding author. E-mail: tochiya@ncc.go.jp

RESULTS

Establishment of a metastatic breast cancer cell line that exhibits homing to bone marrow

We established a breast cancer cell line that exhibited metastatic homing to bone marrow by injecting C.B-17/Icr-scid/scidJc1 mice with MDA-MB-231 cells expressing luciferase and green fluorescent protein (GFP), monitoring metastasis with bioluminescence, and analyzing the bone marrow for metastatic cells (fig. S1A). The resulting clone from the bone marrow was confirmed to be GFP-positive, indicating that these cells originated from the parental cell line (fig. S1B), and was named MDA-MB-231-BM2 (or BM2, for short). Whereas about half the population of the parental MDA-MB-231-luc-D3H2LN-GFP cells exhibited surface abundance of CD24, the bulk of the BM2 clone did not (fig. S1C), indicating that the bulk of the BM2 clone had a characteristic of breast CSCs. In addition, the expression of many genes was similar in BM2 cells and parental cells; however, the expression of genes related to the cell cycle was decreased in BM2 cells compared with the parental cells (fig. S2, A and B).

Coculture of breast cancer cells with BM-MSCs to induce dormancy

The microenvironment plays an important role in tumor development, progression, and metastatic seeding. To determine the effects of BM-MSCs on BM2 cells, we cocultured BM2 cells with BM-MSCs derived from each of four human donors (table S1). We first confirmed that the BM-MSCs were positive for CD73, CD90, and CD105, surface markers of BM-MSCs (fig. S3). BM2 cells were labeled with the lipophilic dye PKH26, which is retained in dormant or slow-cycling cells in culture (*23*). PKH26-labeled BM2 cells were cocultured with BM-MSCs from different donors at ratio of 1 to 1. As a control, a culture of BM2 cells was incubated alone. We confirmed that almost all of the BM2 cells in either culture were positive for PKH26 on day 0 after labeling (fig. S4). Through microscopic analysis 72 hours later, we observed that BM2 cells cocultured with BM-MSCs retained PKH26 labeling more so than did BM2 cells cultured alone (Fig. 1A). Simultaneously, through flow cytometric analysis, we found that the positive-to-negative ratio of PKH26-labeled cells was greater in BM2 cells cocultured with BM-MSCs compared with those cultured in isolation (Fig. 1B). Additionally, we confirmed a change toward a dormant state in BM2 cells cocultured with BM-MSCs with cell cycle analysis, in which trends for the number of cells in the $G_{2/M}$ phase decreased and the number of cells in the G_0/G_1 phase increased in BM2 cells cocultured with BM-MSC compared with BM2 cells cultured alone (Fig. 1C). These findings indicated that a proportion of BM2 cells acquired dormancy after coculture with BM-MSCs.

From among several BM-MSC cultures, we selected a relatively potent line, R14. Using the R14 cell line, we examined the surface abundance of CD44 and CD24 on cocultured BM2 cells to investigate whether CSC characteristics were changed by coculture with BM-MSCs. We found that the number of CD44-negative ($CD44^-$) cells in cocultures markedly increased compared with that in lone BM2 cultures (Fig. 1D), although CD24 surface abundance was not different between the two (Fig. 1E). In addition, $CD44^-$ cells sorted from the cocultured BM2 cells became $CD44^+$ after several weeks of monoculture (Fig. 1F). These findings show that CD44 abundance as a CSC marker on BM2 cells was decreased by coculture with BM-MSCs, suggesting that cell proliferation and migration of BM2 cells might be affected as well as the change of surface abundance of CSC marker.

Different properties of $CD44^-$ cells and $CD44^+$ cells

To investigate whether decreased surface abundance of CD44 after coculture with BM-MSCs was correlated with the finding that the BM2 cell

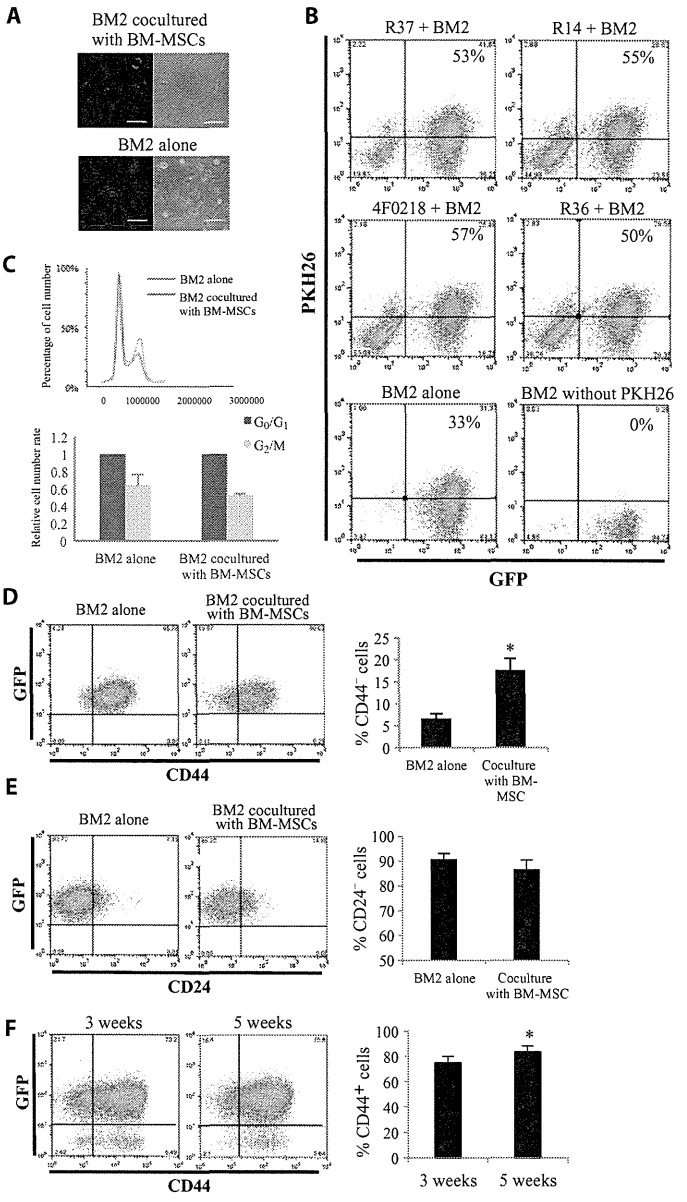

Fig. 1. Acquisition of dormancy in breast CSCs cocultured with BM-MSCs. (A and B) Microscopy (A) and flow cytometry (B) for PKH26 retention in PKH26-labeled BM2 cells cocultured with BM-MSCs for 72 hours compared with BM2 cells cultured alone. Scale bars, 100 μm. Data are representative of three experiments. (C) Cell cycle analyses using Hoechst 33342 in BM2 cells cultured alone or cocultured with R14 BM-MSCs. Data are means ± SE (n = 3; P = 0.20, Student's t test). (D) Flow cytometric analyses of CD44 abundance in BM2 cells cultured alone or cocultured with R14 BM-MSCs (upper panel). Data are means ± SE of three experiments; $^*P < 0.05$, Student's t test. (E) Flow cytometric analyses of CD24 abundance in BM2 cells cultured alone or cocultured with R14 BM-MSCs. (F) $CD44^-$ cells were sorted from BM2 and R14 BM-MSC coculture and BM2 cells cultured alone for up to 5 weeks; flow cytometric analysis of CD44 abundance was performed at 3 or 5 weeks. Data in (E) and (F) are means ± SE of three experiments; (E) P = 0.10, (F) $^*P < 0.05$, Student's t test.

line acquired dormancy, we compared the characteristics of $CD44^-$ cells and $CD44^+$ cells. We sorted BM2 cells cocultured with BM-MSCs into $CD44^-$ and $CD44^+$ populations and confirmed the *CD44* expression status in each using immunocytochemistry and quantitative real-time polymerase chain reaction (qRT-PCR) (fig. S5, A and B). We then examined each population for proliferation, invasive capacity, and drug sensitivity. $CD44^-$ cells had significantly decreased proliferation (Fig. 2A) and a significantly decreased invasion capacity compared with $CD44^+$ cells (Fig. 2B). Furthermore, $CD44^-$ cells were less sensitive to docetaxel, a common breast cancer therapeutic, than $CD44^+$ cells (Fig. 2C). Finally, we confirmed that the global gene expression patterns of the $CD44^+$ and $CD44^-$ BM2 cells were similar, although some genes that encode proteins that influence breast cancer cell dormancy, such as *SRC* (*24*) and *ERBB2* (*25*), were increased and decreased, respectively, in the $CD44^-$ population (fig. S6, A and B). These findings provided evidence that the increased proportion of $CD44^-$ cells in BM2 cultures induced by BM-MSCs was associated with the acquisition of dormancy.

Contribution of BM-MSC–derived exosomes to the acquisition of dormancy in BM2 cells

Next, we investigated how BM-MSCs promoted a dormant phenotype in BM2 cell cultures. We found that culturing BM2 cells in a BM-MSC–conditioned medium increased the number of $CD44^-$ BM2 cells (Fig. 3A), suggesting that a factor secreted by BM-MSCs was responsible for the dormant state of BM2 cells. Therefore, we investigated the role of exosomes derived from BM-MSCs in the dormancy of BM2 cells. We isolated exosomes from R14 BM-MSC–conditioned medium using standard ultracentrifugation. Using phase-contrast electron microscopy and nanoparticle tracking analysis (NTA), we determined that BM-MSC–derived exosomes were about 100 to 200 nm in width, similar to the size of extracellular vesicles (fig. S7A), and physically homogeneous, with most exosomes exhibiting a size of 120 to 160 nm (fig. S7B). Through immunoblotting, we confirmed that the exosomes were positive for the known exosome markers CD9 and CD81 (fig. S7C). Furthermore, using SYTO64 dye, we detected the migration of secreted nucleic acids from BM-MSCs into cocultured BM2 cells (Fig. 3B and fig. S8), and PKH26-labeled exosomes derived from BM-MSCs were taken up by BM2 cells (Fig. 3C and fig. S9). To test whether BM-MSC–derived exosomes could induce dormancy in BM2 cells, we treated PKH26-labeled BM2 cells with exosomes derived from BM-MSCs. After 3 days of incubation, we performed flow cytometry and found that the exosome treatment maintained higher levels of PKH26 abundance on BM2 cells, meaning induction of dormancy in a portion of BM2 cells treated with BM-MSC–derived exosome (Fig. 3D and fig. S10A). In addition, CD44 surface abundance was decreased in BM2 cells treated with BM-MSC–derived exosomes (Fig. 3E and fig. S10B).

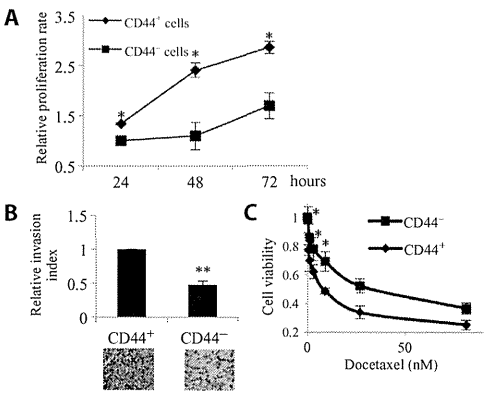

Fig. 2. Phenotypic differences between $CD44^+$ and $CD44^-$ cells. The characteristics of $CD44^+$ and $CD44^-$ cells sorted from BM2 cells by flow cytometry were compared. (A) Cell proliferation normalized to that in $CD44^-$ cells at 24 hours. Each bar represents the mean ± SE ($n = 3$; $^*P < 0.05$). (B) Cell invasion by $CD44^+$ and $CD44^-$ cells normalized to that in $CD44^+$ cells. Data are means ± SE ($n = 3$; $^{**}P < 0.001$ versus $CD44^+$ cells, Student's *t* test). Scale bar, 100 μm. (C) Cell proliferation after docetaxel treatment ($n = 3$; $^*P < 0.05$, Student's *t* test).

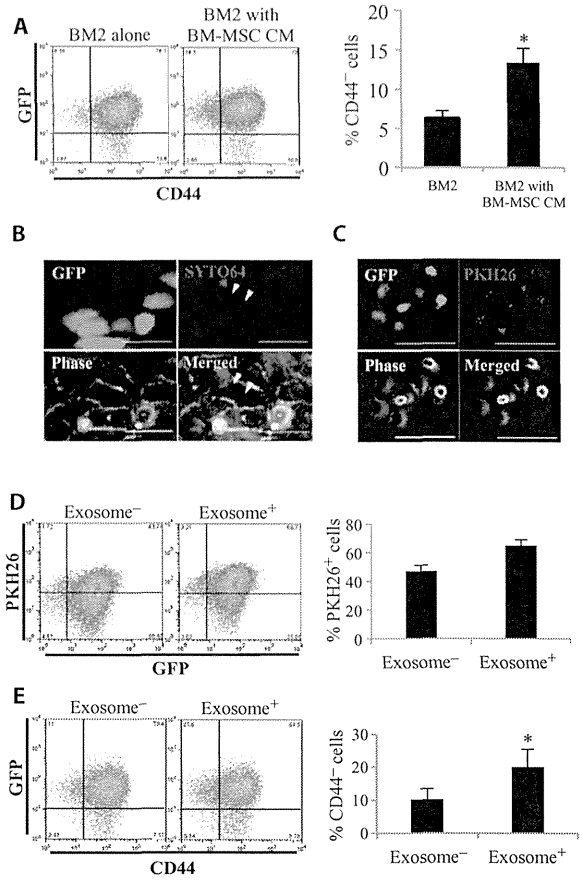

Fig. 3. Induction of a dormant state in BM2 cells by BM-MSC–derived exosomes. (A) Flow cytometric analysis of CD44 abundance in BM2 cells cultured with conditioned medium (CM) derived from R14 BM-MSCs. Each bar represents the mean ± SE ($n = 3$; $^*P < 0.05$, Student's *t* test). (B) BM2 cells were cocultured with SYTO64-labeled R14 BM-MSCs, and images were obtained after 24 hours of coculture. Scale bars, 50 μm. The migration of secreted nucleic acids from BM-MSCs into cocultured BM2 cells was detected (white arrow). (C) PKH26-labeled exosomes derived from R14 BM-MSCs were added to BM2 cells. After incubation for 24 hours, images were obtained. Scale bars, 100 μm. (D) PKH26-labeled BM2 cells were treated with exosomes derived from R14 BM-MSCs or phosphate-buffered saline (PBS). After incubation for 72 hours, PKH26 abundance was analyzed by flow cytometry. Data are means ± SE ($n = 3$; $P = 0.07$, Student's *t* test). (E) R14 BM-MSC–derived exosomes or PBS was added to BM2 cells. After incubation for 1 week, flow cytometry was performed to assess CD44 abundance. Data are means ± SE ($n = 3$; $^*P < 0.05$, Student's *t* test).

Common characteristics between BM2 cells treated with BM-MSC–derived exosomes and CD44⁻ BM2 cells

To investigate the characteristics exhibited by BM2 cells treated with BM-MSC–derived exosomes, we treated the $CD44^+$ fraction of BM2 cells with BM-MSC–derived exosomes or PBS as a control and performed several experiments. First, we examined cell proliferation in $CD44^+$ BM2 cells treated with or without BM-MSC–derived exosomes and found that the $CD44^+$ cells treated with exosomes had significantly decreased cell proliferation (Fig. 4A and fig. S11A) and cell invasion (Fig. 4B and fig. S11B) compared with those cultured alone, although invasion exhibited by cells cultured with R37-dervied exosomes was not significantly decreased. These findings were validated using exosomes derived from BM-MSCs isolated from other volunteers (fig. S11, A and B). To confirm that BM-MSC–derived exosomes could also affect the characteristics of BM2 cells in vivo, BM-MSC–derived exosomes or the same volume of PBS was added to cultures of BM2 cells at days 1 and 4 and incubated for 7 days before being injected into the mammary fat pads of severe combined immunodeficient (SCID) mice. Twenty days after injection, the luciferase activity in tumors resulting from BM2 cell proliferation was lower in the mice implanted with BM-MSC–derived exosome-treated cells than that in controls (Fig. 4C), indicating that the exosomes slowed tumor growth (or tumor formation) by BM2 cells. Additionally, exosome-treated $CD44^+$ BM2 cells exhibited somewhat greater drug resistance compared with cultures lacking exosomes (Fig. 4D and fig. S11C), although the effect of R37-derived exosomes was not statistically significant. These findings suggested that the characteristics of the exosome-treated $CD44^+$ cells were shared by the $CD44^-$ cells in dormant BM2 cells by decreasing surface abundance of CD44 in BM2 cell population.

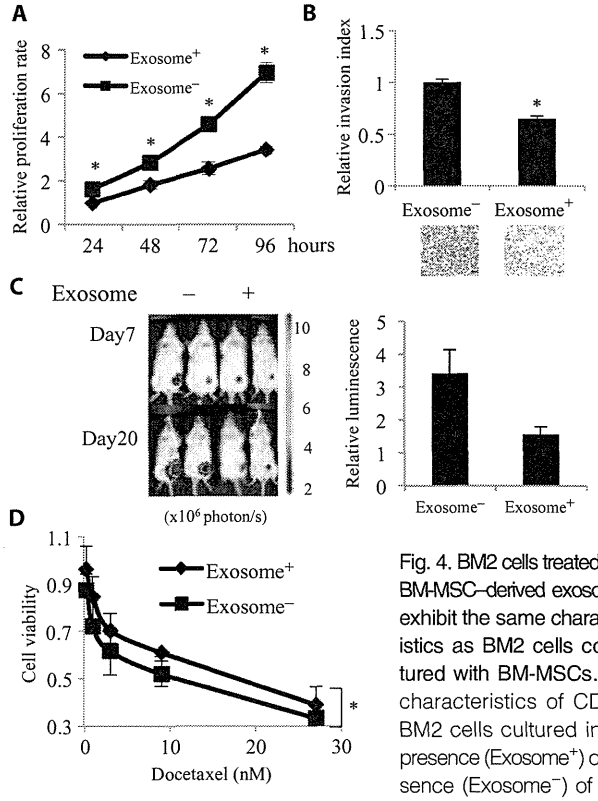

Fig. 4. BM2 cells treated with BM-MSC–derived exosomes exhibit the same characteristics as BM2 cells cocultured with BM-MSCs. The characteristics of $CD44^+$ BM2 cells cultured in the presence ($Exosome^+$) or absence ($Exosome^-$) of R14 BM-MSC–derived exosomes were compared. BM2 cells not cocultured with exosomes were treated with PBS. (A) Cell proliferation in $CD44^+$ BM2 cells cultured with exosomes normalized to that in cells cultured in the absence of exosomes at 24 hours. Data are means ± SE (n = 3; $^*P < 0.01$, Student's t test). (B) Cell invasion by $CD44^+$ BM2 cells cultured with or without exosomes, normalized to the invasion index of cells cultured without exosomes. Data are means ± SE (n = 3; $^*P < 0.05$ versus cells without exosomes, Student's t test). Scale bar, 100 μm. (C) Bioluminescence quantification in an orthotopic xenograft mouse model of tumors derived from $CD44^+$ BM2 cells cultured in the presence or absence of exosomes. Data are means ± SE (n = 5 mice; P = 0.42, Student's t test) compared with $CD44^+$ BM2 cells treated without exosomes at day 20. (D) Proliferation of $CD44^+$ BM2 cells treated with docetaxel alone or in the presence of exosomes (n = 3; $^*P < 0.01$, Student's t test).

Dormancy in BM2 cultures from exosomal miRNAs derived from BM-MSCs

We next explored which aspects of BM-MSC–derived exosomes promoted dormancy in BM2 cells. Because exosomes contain a large number of miRNAs that diversely influence on cells, we hypothesized that miRNAs in the BM-MSC–derived exosomes contributed to the dormant state of BM2 cells through exosome-mediated transfer. We analyzed the miRNA abundance signature in BM-MSC–derived exosomes compared with that in adult fibroblasts as a control and identified 44 miRNAs with a more than twofold increase in expression in R14 BM-MSC–derived exosomes (table S2). Of these, we selected miR-23b on the basis of previous reports showing that miR-23b suppresses cell invasion and migration or that it contributes to cell cycle arrest and the inhibition of cell proliferation (*26*, *27*). Using qRT-PCR, we confirmed that the abundance of *miR-23b* was more than twofold greater in R14 BM-MSC–derived exosomes compared with that in the adult fibroblasts (fig. S12).

To investigate whether miR-23b affected the dormant state of BM2 cells, PKH26-labeled BM2 cells were transfected with ectopic miR-23b or an empty expression vector as a negative control. Overexpression of miR-23b was confirmed by qRT-PCR (fig. S13). Three days after transfection, we found that BM2 cells transfected with miR-23b had a somewhat greater proportion of PKH26-positive cells than those transfected with the control (Fig. 5A). In addition, we investigated whether the overexpression of miR-23b modulated the surface abundance of CD44 in BM2 cell cultures. $CD44^+$ BM2 cells were transfected with miR-23b or the negative control vector. We found that the $CD44^-$ proportion of the cell population increased by 10% upon overexpression of miR-23b (Fig. 5B). These findings indicated that exosomal miR-23b was responsible for the induction of dormancy in BM2 cells. We also found that the $CD44^+$ BM2 cells with miR-23b overexpression had decreased cell proliferation (fig. S14A) and relatively decreased cell invasion compared with the control, although the latter was not statistically significant (fig. S14B). Additionally, we performed an orthotopic injection of miR-23b–transfected BM2 cells into the mammary fat pads of SCID mice. Twelve days later, we found that the luciferase activity in tumors resulting from miR-23b–transfected BM2 cells was somewhat, but not significantly, decreased compared with that in tumors from control cells (Fig. 5C), indicating that miR-23b may decrease cell proliferation in vivo. Together, these results suggested that bone marrow–secreted miR-23b may contribute to the induction of dormancy in disseminated breast cancer cells.

Targets of exosomal miR-23b in BM2 cells

To identify the target of miR-23b that mediated dormancy induction in BM2 cells, we used in silico information (TargetScan and miRanda) to determine that miR-23b targets genes and identified several cell cycle–related genes, including *CCNG1*, *CDC40*, *CDC23*, *CDC6*, *E2F6*, *HDAC7*, and

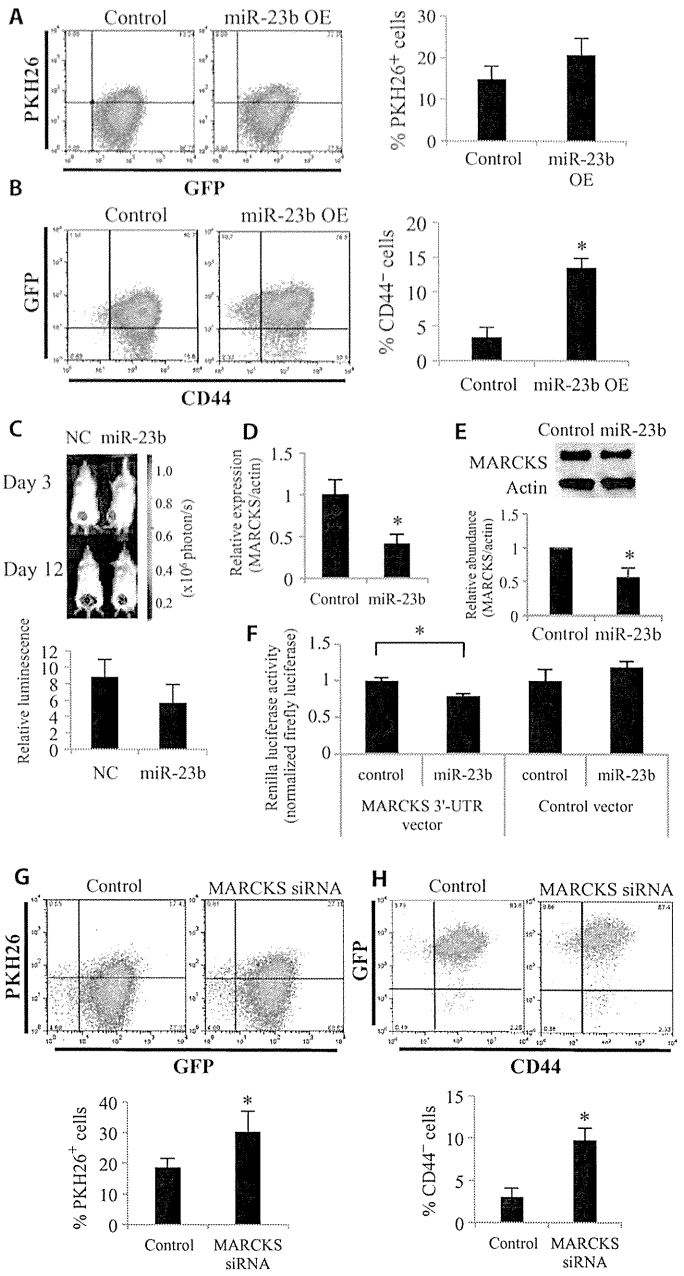

Fig. 5. Suppression of *MARCKS* by miR-23b. (A) Flow cytometric analysis of the PKH26 retention in PKH26-labeled BM2 cells transfected with miR-23b (miR-23b OE) or a negative control vector (control). Data are means ± SE (n = 3; P = 0.08, Student's t test). (B) Flow cytometric analysis of CD44 abundance in $CD44^+$ BM2 cells transfected with miR-23b (miR-23b OE) or negative control (control). Data are means ± SE (n = 3; $^*P < 0.05$, Student's t test). (C) Bioluminescence quantification in an orthotopic xenograft mouse model of tumors derived from miR-23b–overexpressing BM2 cells (miR-23b) (n = 5 tumors) or negative control–transfected cells (NC) (n = 4 tumors). Data are means ± SE (P = 0.60, Student's t test). (D) Expression of *MARCKS* in BM2 cells transfected with miR-23b or a negative control vector (control) was analyzed by qRT-PCR. Data are means ± SE (n = 3; $^*P < 0.05$, Student's t test). (E) Immunoblot analysis of MARCKS against β-actin derived from BM2 cells transfected with miR-23b or control vector. Equal amounts of protein concentration were analyzed by immunoblotting. Data are means ± SE (n = 3; P = 0.04, Student's t test). (F) 3′UTR reporter assay using HEK293 cells. HEK293 cells were cotransfected with hsa-miR-23b or negative control (control) and MARCKS 3′UTR vector or with its control vector. After 48 hours, luciferase activity was measured (n = 8; $^*P <$ 0.004, Student's t test). (G and H) PKH26-labeled BM2 cells were transfected with MARCKS siRNA or a control siRNA (control). PKH26 retention (G) and CD44 abundance (H) were analyzed by flow cytometry 72 hours later. Data are means ± SE (n = 3; $^*P < 0.05$, Student's t test).

YWHAG (table S3). In particular, miR-23b targeted *MARCKS*, which encodes myristoylated alanine-rich C kinase substrate. MARCKS promotes cell motility and cycling and is implicated in the pathogenesis of metastatic cancers (*28*). Using qRT-PCR, we found that *MARCKS* expression in BM2 cells transfected with miR-23b was significantly decreased compared with cells transfected with a negative control (Fig. 5D). In addition, we confirmed that the abundance of MARCKS was decreased in miR-23b–transfected BM2 cells compared with controls (Fig. 5E), and that miR-23b bound directly to the 3′ untranslated region (3′UTR) of *MARCKS* and suppressed its transcription in human embryonic kidney (HEK) 293 cells (Fig. 5F). Furthermore, we analyzed the expression of *miR-23b* in BM2 cells treated with BM-MSC–derived exosomes and found that the expression of *miR-23b* was significantly increased and *MARCKS* expression significantly decreased in BM2 cells treated with exosomes compared with untreated cells (fig. S15). Finally, we performed a flow cytometric analysis of BM2 cells transfected with a small interfering RNA (siRNA) against *MARCKS* or a negative control siRNA. We found that the MARCKS knockdown in BM2 cells (fig. S16) induced dormancy as inferred from an increase in the proportion of PKH26-positive BM2 cells and decreased the surface abundance of CD44 compared with those transfected with the control (Fig. 5, G and H). Additionally, $CD44^+$ BM2 cells transfected with MARCKS siRNA had decreased cell proliferation and invasion (fig. S17, A and B) compared with those transfected with the control. Together, these findings demonstrated that exosomal transfer of miR-23b from BM-MSCs decreased *MARCKS* expression in BM2 cells, promoting the acquisition of dormancy.

BM-MSCs adjacent to breast cancer cells in the bone marrow of breast cancer patients

To corroborate our findings in humans, we examined clinical samples from breast cancer patients in whom cancer cells had metastasized to bone marrow. We performed immunohistochemical analysis of bone marrow specimens from three patients with breast cancer metastases to bone marrow to examine the relationship between breast cancer cells and BM-MSCs. In the bone marrow, BM-MSCs were observed among or adjacent to clusters of breast cancer cells (Fig. 6A), confirming that BM-MSCs coexisted with breast cancer cells in bone marrow in breast cancer patients. Using laser capture microdissection, we isolated cancer cells from both bone marrow and primary breast tissue from 10 patients who presented with breast cancer metastasis to the bone marrow. We found that the expression of *miR-23b* trended higher and that of *MARCKS* trended lower in the cancer cells isolated from bone marrow compared with those from primary breast tissue (Fig. 6B), although neither was statistically significant. The patient data generally support our findings in cells and mice, and suggest that this mechanism may contribute to the dormant phenotype of disseminated breast cancer cells in the bone marrow.

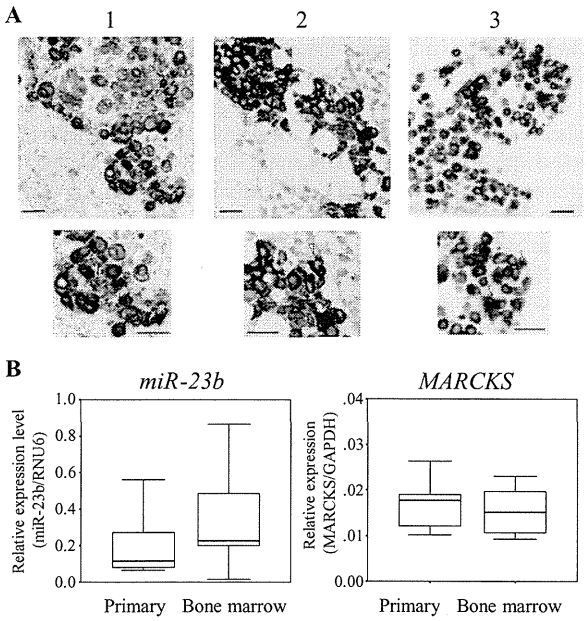

Fig. 6. Analysis of clinical samples from patients with breast cancer metastasis to bone marrow. (A) Immunohistochemical analyses of bone marrow from three patients (numbered 1, 2, and 3) with breast cancer that metastasized to bone marrow were performed. CD105 (brown) and cytokeratin (purple) stainings indicate BM-MSCs and breast cancer cells, respectively. (B) miR-23b and *MARCKS* expression in breast cancer cells in primary lesions and in bone marrow (n = 10; miR-23b, P = 0.13; *MARCKS*, P = 0.87; Wilcoxon test).

DISCUSSION

The microenvironment contains many factors and cell types, such as immune cells, stromal cells, and endothelial cells, that influence cancer progression (*29*). Cancer cells and surrounding noncancerous cells interact by secreting exosomes. It has been demonstrated that exosomes derived from noncancerous cells influence cancer progression and metastasis. Fibroblast-secreted exosomes promote breast cancer cell migration by activating autocrine Wnt–PCP (planar cell polarity) signaling in breast cancer cells (*21*), and BM-MSC–derived exosomes facilitate the progression of multiple myelomas through the transfer of miR-15a (*22*). Moreover, several studies have reported that cancer cell–derived exosomes contribute to cancer progression by inducing changes in surrounding noncancerous cells. For example, melanoma-secreted exosomes enable bone marrow progenitor cells to travel to secondary organs (*20*), and Kosaka *et al.* (*18*) showed that exosomes secreted from breast cancer cells drove endothelial cells to promote angiogenesis, enabling cancer metastasis. Furthermore, neutrophil infiltration, which promotes tumor formation and metastasis, was found to be promoted by cancer cell–derived exosomes (*19*). Thus, there are increasing reports about the role of exosomes in cancer biology. Here, we demonstrated that BM-MSCs play an important role in inducing dormancy in $CD44^+/CD24^-$ breast CSCs in bone marrow through the transfer of a cell cycle inhibitory miRNA, indicating that breast CSCs are maintained by surrounding noncancerous BM-MSCs.

Some reports indicated that a vascular niche composed of endothelial cells maintains CSC "stemness" in skin tumors (*13*) and brain tumors (*14*). Ghajar *et al.* (*30*) also determined that a stable microvasculature formed a niche for cancer cell dormancy, although they did not refer to CSCs. These findings suggested that CSCs are maintained by a microenvironment similar to those of normal stem cells, such as hematopoietic stem cells and neural stem cells (*6*, *31*). Here, we identified BM-MSCs, which constitute niche-regulating hematopoietic stem cells, promote breast CSC dormancy. Although it is believed that bone marrow functions as a reservoir for disseminated tumor cells and that metastasis to secondary organs occurs because of the recirculation of disseminated tumor cells from bone marrow, the precise mechanisms remain unclear. It was reported that periostin, a component of the extracellular matrix derived from stromal cells, was required for the colonization of breast CSCs after their metastasis to secondary organs (*32*). Our study demonstrated mechanisms of maintaining breast CSCs in a dormant state in bone marrow that may occur before their metastatic growth there or in target organs. In addition, we found that the surface abundance of CD44, a characteristic marker of breast CSCs, was decreased in BM2 cultures that acquired dormant phenotypes. It is reported that $CD44^+/CD24^-$ cells are breast CSCs, defined largely by their tumorigenicity in mouse studies. However, although tumorigenicity is considered a feature of CSCs (*33*), it does not indicate dormancy in stem cells. It is possible that changes in CD44 surface abundance are reversible and that cells regain tumorigenicity with time or in response to conditions in the microenvironment.

In addition, we discovered that the effects of BM-MSCs on breast CSCs were attributable to the transfer of miRNAs from BM-MSCs to breast CSCs through exosomes. We revealed that exosomal miR-23b promoted dormancy and decreased CD44 surface abundance in breast cancer cells. In agreement with our study, miR-23b induces cell cycle arrest in glioma CSCs and suppresses glioma cell migration and invasion (*26*, *27*). We identified *MARCKS* as a target gene of miR-23b through in silico analysis. *MARCKS* expression is associated with the pathogenesis of metastatic cancers, and the inhibition of *MARCKS* expression reduces cell invasion and induces cell cycle arrest in colon cancer (*28*). Using qRT-PCR and immunoblotting, we confirmed that the *MARCKS* expression in BM2 cells transfected with miR-23b was significantly decreased compared with the control. Exosomal miR-23b was transferred to BM2 cells, where it suppressed the *MARCKS* expression. However, in our study, whereas xenografts derived from exosome-treated BM2 cells exhibited substantially decreased tumor growth, xenografts derived from BM2 cells overexpressing miR-23b did not exhibit the same degree of proliferative inhibition, suggesting that factors additional to miR-23b contribute to this effect. Therefore, we conclude that exosomal transfer of miR-23b and its suppression of *MARCKS* is one of the mechanisms contributing to cell cycle suppression and dormancy in breast CSCs.

Here, we focused on how cancer cells maintain a dormant state before cancer recurrence, and our findings provide new insights into that issue. From this viewpoint, it is feasible that the mechanism by which cancer cells switch from a dormant state to a proliferative state should function when cancer recurs; however, we did not address this point in this study. Further research is needed to clarify that mechanism. Because exosomes include not only miRNAs but also many types of mRNAs, proteins, and cytokines (*16*, *17*), it is possible that certain proteins function additively. In addition, in this study, the induction of dormancy occurred in only about 10% of cancer cells, suggesting that although miR-23b–mediated suppression of *MARCKS* contributes, there are likely multiple mechanisms that cooperate to promote dormancy in breast CSCs. Nonetheless, our findings suggest that targeting molecules secreted through exosomes from metastatic niches may prevent or delay cancer recurrence.

MATERIALS AND METHODS

Cell culture and establishment of a bone marrow–metastatic breast cancer cell line

Donor information for the human BM-MSC lines R14, R36, R37 (RIKEN), and 4F0218 (Cambrex) is provided in table S1. BM-MSCs were routinely

cultured in MesenPRO RS medium (Invitrogen) containing 2% serum and supplemented with 2 mM GlutaMAX and an antibiotic-antimycotic [penicillin (100 U/ml), streptomycin (100 μg/ml), and amphotericin B (0.25 μg/ml)] (Invitrogen) at 37°C in 5% CO_2. All BM-MSCs were used by the 10th passage. For the coculture of breast cancer cells with BM-MSCs, equal proportions of BM2 cells and BM-MSCs were cocultured in MesenPRO RS medium as described for BM-MSCs. To obtain BM-MSC–conditioned medium, the medium was collected after 2 to 3 days of incubation with the relevant BM-MSC line and centrifuged at 2000*g* for 10 min at 4°C. Supernatant was filtered through a 0.22-μm filter unit (Millipore) to thoroughly remove the cellular debris. Conditioned medium was then ultracentrifuged at 110,000*g* for 70 min at 4°C. Pellets were washed with 11 ml of PBS, ultracentrifuged again, and resuspended in PBS. The protein content of the exosome fraction was measured using the Micro BCA Protein Assay Kit (Thermo Scientific). To track metastasis and establish a bone marrow–metastatic cell line, lentiviral infection of MDA-MB-231-luc-D3H2LN cells (Xenogen) was performed with the pGreenPuro Scramble Hairpin Control (construct MZIP000-PA-1, System Biosciences) to establish breast cancer cells that stably expressed both firefly luciferase and a GFP cloned from copepod *Pontellina plumata* (cop-GFP, also known as ppluGFP2). These cells, which we called MDA-MB-231-luc-D3H2LN-GFP, were cultured in RPMI 1640 containing 10% heat-inactivated fetal bovine serum (FBS) and the antibiotic-antimycotic (above) at 37°C in 5% CO_2. The left heart ventricle of 8-week-old female C.B-17/Icr-scid/scidJc1 mice (Crea Japan) was injected with 1×10^5 MDA-MB-231-luc-D3H2LN-GFP cells suspended in 100 μl of PBS. The subsequent development of metastasis was monitored by injecting luciferin into the mice and measuring bioluminescence using an IVIS imaging system and Living Image 2.50 analysis software (Xenogen). On day 10, bioluminescence was detected in the bilateral legs of a mouse that had received an intracardiac injection. The mouse was sacrificed, and bone marrow was extracted from the legs, cultured in RPMI 1640 as described for the parental MDA-MB-231-luc-D3H2LN-GFP cell line above, and microscopically analyzed for GFP-positive cells. An MDA-MB-231-luc-D3H2LN-GFP cell was cultured under Zeocin selection to establish clones, which we called BM2 cells, cultured in RPMI 1640 as described above for the parental line.

Patient samples

Human bone marrow tissue samples were derived from breast cancer patients treated at the National Cancer Center Hospital. Samples were fixed in formalin, embedded in paraffin, and sectioned for use in microscopic analysis and laser capture microdissection. This study was approved by the Institutional Review Board.

Cell proliferation assay

Cells (3000) were seeded into each well of a 96-well plate and either untreated or treated as indicated in the figures. To assess the effects of exosomal transfer on docetaxel sensitivity, cells were treated with docetaxel for 2 days. Cell viability as a measure of relative proliferation in an MTS [3-(4,5-dimethylthiazol-2-yl)-5-(3-carboxymethoxyphenyl)-2-(4-sulfophenyl)-2-(4-sulfophenyl)-2*H*-tetrazolium] assay was determined on the indicated days using the Cell Counting Kit-8 (Dojindo) according to the manufacturer's instructions, and the absorbance at 450 nm was measured using an EnVision Multilabel Plate Reader (PerkinElmer, Wallac Oy). $CD44^+$ BM2 cells were used for the exosome experiments, and 1 μg of exosomes or PBS at equal volume was added to each well daily.

Transwell invasion assay

The invasion capacity of BM2 cells was assayed in 24-well BioCoat Matrigel 8-μm invasion chambers according to the manufacturer's protocol (Becton Dickinson). Briefly, 1×10^5 cells in serum-free RPMI 1640 medium were plated in the upper chamber. The bottom chamber contained 10% FBS as a chemoattractant. Noninvasive cells were removed with a cotton swab 22 hours later. The cells that migrated through the membrane and adhered to the lower surface of the membrane were fixed with methanol and stained with Diff-Quick Staining Kit. For quantification, the cells were counted under a microscope in four random fields. All assays were performed in triplicate. The data are presented as the percentage invasion through the Matrigel matrix and membrane relative to the migration through the control membrane. In the examination of exosomes, after $CD44^+$ cells were plated in the upper chamber, 1 μg of exosomes derived from BM-MSCs was added to each chamber.

Cell cycle analyses

BM2 cells and BM-MSCs were either cocultured or cultured separately for 72 hours, then fixed with 4% formaldehyde (Sigma-Aldrich) and washed twice in PBS. The cell nuclei were stained with Hoechst 33342 (1:2000, Invitrogen), and the cells were incubated for 15 min. Images were acquired using a 10× water immersion objective and the nonconfocal ultraviolet channel on an Opera high-content screening system (PerkinElmer).

Cell sorting and flow cytometric analyses

BM2 cells were labeled with a PKH26 Red Fluorescent Labeling Kit (Sigma-Aldrich) according to the manufacturer's protocol and cocultured with BM-MSCs. After 72 hours of coculture, the cells were suspended in their culture medium and subjected to flow cytometric analyses using a JSAN cell sorter (Bay Bioscience). At least 1 million cells were pelleted by centrifugation at 180*g* for 5 min at 4°C. BM2 cells were cocultured with BM-MSCs transfected with miR-23b, treated with BM-MSC–conditioned medium, or 3 μg of exosomes. After 7 days in culture (or 3 days for the transfection of miRNAs), the cells were suspended as described above with 5 μl of a monoclonal mouse antibody against human CD44–allophycocyanin (APC) (clone G44-26, BD Pharmingen) or 10 μl of a monoclonal mouse antibody against human CD24-APC (clone ML5, BioLegend) and incubated for 30 min at 4°C.

Isolation of miRNAs

Total RNA was extracted from cultured cells using the QIAzol reagent and the miRNeasy Mini Kit (Qiagen), and total RNA was extracted from clinical specimens using the RecoverAll Total Nucleic Acid Isolation Kit (Ambion) according to the manufacturer's protocols.

Quantitative real-time polymerase chain reaction

qRT-PCR was performed as previously described (*34*). miRNA expression was quantified using TaqMan miRNA assays (Applied Biosystems). PCR was performed in 96-well plates using the 7300 Real-Time PCR System (Applied Biosystems). All reactions were performed in triplicate. *hRNU6* was used as an invariant control for assessing the expression of cellular miRNAs. The TaqMan probes for *hsa-miR-23b* (*miR-23b*) and *hRNU6* were purchased from Applied Biosystems.

Microarrays

Raw and normalized microarray data are available in the Gene Expression Omnibus (GEO) database (accession numbers GSE57921 and GSE58027). Total RNA was extracted from cultured cells using the QIAzol reagent and the miRNeasy Mini Kit (Qiagen). RNA quantity and quality were determined using a NanoDrop ND-1000 spectrophotometer (Thermo Fisher Scientific Inc.) and an Agilent Bioanalyzer (Agilent Technologies), as recommended. Total RNA was amplified and labeled with cyanine 3 (Cy3) using Low Input Quick Amp Labeling Kit, one-color (Agilent Technologies)

following the manufacturer's instructions. Briefly, 100 ng of total RNA was reversed-transcribed to double-strand complementary DNA (cDNA) using a poly dT-T7 promoter primer. Primer, template RNA, and quality-control transcripts of known concentration and quality were first denatured at 65°C for 10 min and incubated for 2 hours at 40°C with 5× first strand buffer, 0.1 M dithiothreitol, 10 mM deoxynucleotide triphosphate mix, and AffinityScript RNase Block Mix. The AffinityScript enzyme was inactivated at 70°C for 15 min. cDNA products were then used as templates for in vitro transcription to generate fluorescent complementary RNA (cRNA). cDNA products were mixed with a transcription master mix in the presence of T7 RNA polymerase and Cy3-labeled CTP (cytidine 5′-triphosphate) and incubated at 40°C for 2 hours. Labeled cRNA was purified using RNeasy Mini Spin Columns (Qiagen) and eluted in 30 μl of nuclease-free water. After amplification and labeling, cRNA quantity and cyanine incorporation were determined using a NanoDrop ND-1000 spectrophotometer and an Agilent Bioanalyzer. For each hybridization, 0.60 μg of Cy3-labeled cRNA was fragmented and hybridized at 65°C for 17 hours to an Agilent SurePrint G3 Human GE v2 8x60K Microarray (design ID: 039494). After washing, microarrays were scanned using an Agilent DNA microarray scanner. Intensity values of each scanned feature were quantified using Agilent Feature Extraction software version 10.7.3.1, which performs background subtractions. We only used features that were flagged as no errors (present flags) and excluded features that were not positive, not significant, not uniform, not above background, saturated, and population outliers (marginal and absent flags). Normalization was performed with Agilent GeneSpring GX version 12.6.1 (per chip: normalization to 75th percentile shift; per gene: normalization to median of all samples). There are a total of 50,599 probes on Agilent SurePrint G3 Human GE v2 8x60K Microarray (design ID: 039494) without control probes. The altered transcripts were quantified using the comparative method. We applied ≥1.2-fold change in signal intensity to identify the significant differences of gene expression in this study.

Transient miRNA transfection

Synthetic hsa-miR-23b was obtained from Bonac. The AllStars Negative Control siRNA was purchased from Qiagen. The transfection of miRNA and siRNA was accomplished using the DharmaFECT 1 transfection reagent (Thermo Fisher Scientific) according to the manufacturer's protocol. The *hsa-miR-23b* sequences were (5′ to 3′) UGGGUUCCUGGCAUGCUGAUUU (sense) and AUCACAUUGCCAGGGAUUAC (antisense).

Immunohistochemistry

Specimens were formalin-fixed and paraffin-embedded, and 4-μm-thick sections were prepared for immunohistochemistry, performed with antibodies against the BM-MSC marker CD105 (clone SN6, Abcam) and an epithelial marker cytokeratin (clone AE1/AE3, Dako). The sections were deparaffinized and incubated first with the CD105 antibody at room temperature for 1 hour, incubated with a peroxidase-conjugated secondary antibody, and visualized with diaminobenzidine tetrahydrochloride and hydrogen peroxide (CSA II, Dako). Sections were subjected to antigen retrieval by being autoclaved in sodium citrate buffer (pH 6.0) for 10 min at 121°C and allowed to cool to room temperature. Slides were then incubated with a cytokeratin antibody at room temperature for 1 hour, and then incubated with a dextran polymer reagent combined with secondary antibodies and peroxidase (EnVision Plus, Dako) for 2 hours at room temperature. Specific antigen-antibody reactions were visualized using the Vector VIP peroxidase (HRP) Substrate kit.

Immunoblot analysis

Exosomes were lysed in a 2% SDS buffer, and equal amounts of protein were loaded onto an SDS–polyacrylamide gel and transferred onto polyvinylidine difluoride membranes (Bio-Rad Laboratories). Antibodies against CD9 (1:200, Santa Cruz Biotechnology), CD81 (1:200, Santa Cruz Biotechnology), MARCKS (1:5000, Abcam), and β-actin (1:1000, Millipore) were used as primary antibodies. CD9 and CD81 abundance was assessed in nonreducing conditions. As secondary antibodies, HRP (horseradish peroxidase)–linked antibodies against mouse and rabbit immunoglobulin G (GE Healthcare) were used at a dilution of 1:5000. Bound antibodies were visualized by chemiluminescence, and images were analyzed using a LuminoImager (LAS-3000, Fujifilm Inc.).

Nanoparticle tracking analysis

NTA of exosomes resuspended in PBS and further diluted for analysis was performed with the NanoSight LM10-HS system per manufacturer's protocol.

Confocal microscopy

Confocal microscopy was performed with an Olympus FV10i laser scanning microscope. The filters used were 489 to 510 nm (for GFP), 551 to 567 nm (for PKH26), and 599 to 619 nm (for SYTO64).

Phase-contrast transmission electron microscopy

BM-MSC–derived exosomes were visualized using phase-contrast transmission electron microscopy performed by Terabase Inc.

SYTO64-labeled miRNA transfer

BM-MSCs were incubated at 37°C for 7 hours in the presence of 1 μM SYTO64-labeled conditioned medium, the medium was discarded, and the BM-MSCs were washed twice with PBS to remove excess dye. BM2 cells were added to the dish in which BM-MSCs were seeded, and the cells were incubated at 37°C for 24 hours.

PKH26-labeled exosome transfer

Purified exosomes derived from BM-MSCs were labeled with the PKH26 Red Fluorescent Labeling Kit (Sigma). Exosomes were incubated with 2 μM PKH26 for 5 min, washed four times through a 100-kD filter (Microcon YM-100, Millipore) to remove excess dye, and incubated with BM2 cells at 37°C.

Establishment of stable cell lines

Stable BM2 cell lines expressing *miR-23b* were generated by selection with puromycin (2 μg/ml). BM2 cells at 90% confluency were transfected with an hsa-miR-23b expression vector in 24-well dishes using the Lipofectamine LTX Reagent in accordance with the manufacturer's instructions (Life Technologies). Cells were replated in a 10-cm dish 12 hours after transfection, followed by selection with puromycin for 3 weeks. Ten surviving single colonies were picked from each transfectant and cultured for an additional 2 weeks. The cells expressing the largest amount of *miR-23b* among the transfectants were considered to stably express miR-23b.

3′UTR reporter assay plasmid constructs

A 729–base pair fragment from the 3′UTR of *MARCKS*, which contained the predicted target sequences of miR-23b (located at positions 1210 to 1216 and 1654 to 1660 of the *MARCKS* 3′UTR), was cloned by PCR from total RNA isolated from MDA-MB-231 cells. A 3′ polyadenylate overhang was added to the PCR products after 15 min of regular Taq polymerase treatment at 72°C. The PCR products were cloned into a pGEM-T Easy vector (Promega) and ligated into the Not I site of the 3′UTR of the *Rennila* luciferase gene in the psiCHECK-2 plasmid (Promega). The *miR-23b* primer sequences were (5′ to 3′) TGGAGAAGCTTTGACCAATTT (forward) and AAGGCCCATGAACTGACATC (reverse). HEK293 cells were cultured overnight

in 96-well tissue culture plates at densities of 1×10^4 cells per well, respectively, and each construct was cotransfected with hsa-miR-23b using the DharmFECT Duo Transfection Reagent (Thermo Fisher Scientific). The cells were harvested 48 hours after transfection, and the *Rennila* luciferase activity was measured and normalized to the firefly luciferase activity. All assays were performed in triplicate and were repeated at least three times; representative results are shown.

Tumorigenicity assay in SCID mice

BM2 cells (20,000) were seeded into six-well plates, and 3 μg of BM-MSC–derived exosomes or the same amount of PBS was added to each well on days 1 and 4. Five-week-old female C.B-17/Icr-scid/scidJc1 mice (Crea Japan) received mammary fat pad 100-μl injections of PBS containing 1×10^5 BM2 cells that had been cultured with R14 BM-MSC–derived exosomes or PBS for 7 days. Tumor growth was monitored by injecting mice with luciferin and measuring the bioluminescence using an IVIS imaging system (Xenogen). The data were analyzed using Living Image 2.50 software (Xenogen). All experimental protocols involving animals were approved by the Institute for Laboratory Animal Research, National Cancer Center Research Institute.

Statistical analyses

The data presented in bar graphs are means ± SE of at least three independent experiments. The statistical analyses were performed with Student's *t* test or Wilcoxon test. $P < 0.05$ was considered to be statistically significant.

SUPPLEMENTARY MATERIALS

www.sciencesignaling.org/cgi/content/full/7/332/ra63/DC1

Fig. S1. Establishment of a line of breast cancer cells that metastasized to bone marrow.
Fig. S2. Gene expression array in BM2 and parental cells.
Fig. S3. Surface marker profiles of BM-MSCs from human donors.
Fig. S4. Flow cytometric analysis of PKH26 labeling in BM2 cultures.
Fig. S5. CD44 expression and surface abundance on sorted $CD44^+$ and $CD44^-$ cells.
Fig. S6. Gene expression array in $CD44^+$ or $CD44^-$ BM2 cells.
Fig. S7. Characterization of BM-MSC–derived exosomes.
Fig. S8. Images of BM2 cells cocultured with SYTO64-labeled BM-MSCs.
Fig. S9. Images of BM2 cells cocultured with PKH26-labeled exosomes.
Fig. S10. Flow cytometry of BM2 cells cultured with BM-MSC–derived exosomes.
Fig. S11. Proliferation and invasive behavior of BM2 cells cultured with BM-MSC–derived exosomes.
Fig. S12. Expression of *miR-23b* in exosomes derived from BM-MSCs or fibroblasts.
Fig. S13. Overexpression of miR-23b in BM2 cells.
Fig. S14. Proliferation and invasive behavior of BM2 cells overexpressing miR-23b.
Fig. S15. Effect of exosomes on *miR-23b* and *MARCKS* expression in BM2 cells.
Fig. S16. Knockdown of MARCKS in BM2 cells.
Fig. S17. Proliferation and invasive behavior in MARCKS-deficient BM2 cells.
Table S1. Donor information for BM-MSCs.
Table S2. miRNAs that were increased in BM-MSC exosomes.
Table S3. Predicted miR-23b target genes.
Table S4. Expression analysis in BM2 cells.

REFERENCES AND NOTES

1. National Cancer Center for Cancer Control and Information Services, Japan, Cancer mortality (1958–2011). Vital Statistics Japan (Ministry of Health, Labour and Welfare), (2011).
2. J. M. Kurtz, J. M. Spitalier, R. Amalric, Late breast recurrence after lumpectomy and irradiation. *Int. J. Radiat. Oncol. Biol. Phys.* **9**, 1191–1194 (1983).
3. S. Braun, F. D. Vogl, B. Naume, W. Janni, M. P. Osborne, R. C. Coombes, G. Schlimok, I. J. Diel, B. Gerber, G. Gebauer, J. Y. Pierga, C. Marth, D. Oruzio, G. Wiedswang, E. F. Solomayer, G. Kundt, B. Strobl, T. Fehm, G. Y. Wong, J. Bliss, A. Vincent-Salomon, K. Pantel, A pooled analysis of bone marrow micrometastasis in breast cancer. *N. Engl. J. Med.* **353**, 793–802 (2005).
4. M. Balic, H. Lin, L. Young, D. Hawes, A. Giuliano, G. McNamara, R. H. Datar, R. J. Cote, Most early disseminated cancer cells detected in bone marrow of breast cancer patients have a putative breast cancer stem cell phenotype. *Clin. Cancer Res.* **12**, 5615–5621 (2006).
5. K. Pantel, C. Alix-Panabières, S. Riethdorf, Cancer micrometastases. *Nat. Rev. Clin. Oncol.* **6**, 339–351 (2009).
6. M. J. Kiel, O. H. Yilmaz, T. Iwashita, O. H. Yilmaz, C. Terhorst, S. J. Morrison, SLAM family receptors distinguish hematopoietic stem and progenitor cells and reveal endothelial niches for stem cells. *Cell* **121**, 1109–1121 (2005).
7. L. M. Calvi, G. B. Adams, K. W. Weibrecht, J. M. Weber, D. P. Olson, M. C. Knight, R. P. Martin, E. Schipani, P. Divieti, F. R. Bringhurst, L. A. Milner, H. M. Kronenberg, D. T. Scadden, Osteoblastic cells regulate the haematopoietic stem cell niche. *Nature* **425**, 841–846 (2003).
8. F. Arai, A. Hirao, M. Ohmura, H. Sato, S. Matsuoka, K. Takubo, K. Ito, G. Y. Koh, T. Suda, Tie2/Angiopoietin-1 signaling regulates hematopoietic stem cell quiescence in the bone marrow niche. *Cell* **118**, 149–161 (2004).
9. J. Zhang, C. Niu, L. Ye, H. Huang, X. He, W. G. Tong, J. Ross, J. Haug, T. Johnson, J. Q. Feng, S. Harris, L. M. Wiedemann, Y. Mishina, L. Li, Identification of the haematopoietic stem cell niche and control of the niche size. *Nature* **425**, 836–841 (2003).
10. T. Sugiyama, H. Kohara, M. Noda, T. Nagasawa, Maintenance of the hematopoietic stem cell pool by CXCL12-CXCR4 chemokine signaling in bone marrow stromal cell niches. *Immunity* **25**, 977–988 (2006).
11. S. Yamazaki, H. Ema, G. Karlsson, T. Yamaguchi, H. Miyoshi, S. Shioda, M. M. Taketo, S. Karlsson, A. Iwama, H. Nakauchi, Nonmyelinating Schwann cells maintain hematopoietic stem cell hibernation in the bone marrow niche. *Cell* **147**, 1146–1158 (2011).
12. S. Méndez-Ferrer, T. V. Michurina, F. Ferraro, A. R. Mazloom, B. D. Macarthur, S. A. Lira, D. T. Scadden, A. Ma'ayan, G. N. Enikolopov, P. S. Frenette, Mesenchymal and haematopoietic stem cells form a unique bone marrow niche. *Nature* **466**, 829–834 (2010).
13. B. Beck, G. Driessens, S. Goossens, K. K. Youssef, A. Kuchnio, A. Caauwe, P. A. Sotiropoulou, S. Loges, G. Lapouge, A. Candi, G. Mascre, B. Drogat, S. Dekoninck, J. J. Haigh, P. Carmeliet, C. Blanpain, A vascular niche and a VEGF–Nrp1 loop regulate the initiation and stemness of skin tumours. *Nature* **478**, 399–403 (2011).
14. C. Calabrese, H. Poppleton, M. Kocak, T. L. Hogg, C. Fuller, B. Hamner, E. Y. Oh, M. W. Gaber, D. Finklestein, M. Allen, A. Frank, I. T. Bayazitov, S. S. Zakharenko, A. Gajjar, A. Davidoff, R. J. Gilbertson, A perivascular niche for brain tumor stem cells. *Cancer Cell* **11**, 69–82 (2007).
15. A. E. Karnoub, A. B. Dash, A. P. Vo, A. Sullivan, M. W. Brooks, G. W. Bell, A. L. Richardson, K. Polyak, R. Tubo, R. A. Weinberg, Mesenchymal stem cells within tumour stroma promote breast cancer metastasis. *Nature* **449**, 557–563 (2007).
16. H. Valadi, K. Ekström, A. Bossios, M. Sjöstrand, J. J. Lee, J. O. Lötvall, Exosome-mediated transfer of mRNAs and microRNAs is a novel mechanism of genetic exchange between cells. *Nat. Cell Biol.* **9**, 654–659 (2007).
17. J. Skog, T. Würdinger, S. van Rijn, D. H. Meijer, L. Gainche, M. Sena-Esteves, W. T. Curry Jr., B. S. Carter, A. M. Krichevsky, X. O. Breakefield, Glioblastoma microvesicles transport RNA and proteins that promote tumour growth and provide diagnostic biomarkers. *Nat. Cell Biol.* **10**, 1470–1476 (2008).
18. N. Kosaka, H. Iguchi, K. Hagiwara, Y. Yoshioka, F. Takeshita, T. Ochiya, Neutral Sphingomyelinase 2 (nSMase2)-dependent exosomal transfer of angiogenic microRNAs regulate cancer cell metastasis. *J. Biol. Chem.* **288**, 10849–10859 (2013).
19. A. Bobrie, S. Krumeich, F. Reyal, C. Recchi, L. F. Moita, M. C. Seabra, M. Ostrowski, C. Théry, Rab27a supports exosome-dependent and -independent mechanisms that modify the tumor microenvironment and can promote tumor progression. *Cancer Res.* **72**, 4920–4930 (2012).
20. H. Peinado, M. Alečković, S. Lavotshkin, I. Matei, B. Costa-Silva, G. Moreno-Bueno, M. Hergueta-Redondo, C. Williams, G. García-Santos, C. Ghajar, A. Nitadori-Hoshino, C. Hoffman, K. Badal, B. A. Garcia, M. K. Callahan, J. Yuan, V. R. Martins, J. Skog, R. N. Kaplan, M. S. Brady, J. D. Wolchok, P. B. Chapman, Y. Kang, J. Bromberg, D. Lyden, Melanoma exosomes educate bone marrow progenitor cells toward a pro-metastatic phenotype through MET. *Nat. Med.* **18**, 883–891 (2012).
21. V. Luga, L. Zhang, A. M. Viloria-Petit, A. A. Ogunjimi, M. R. Inanlou, E. Chiu, M. Buchanan, A. N. Hosein, M. Basik, J. L. Wrana, Exosomes mediate stromal mobilization of autocrine Wnt-PCP signaling in breast cancer cell migration. *Cell* **151**, 1542–1556 (2012).
22. A. M. Roccaro, A. Sacco, P. Maiso, A. K. Azab, Y. T. Tai, M. Reagan, F. Azab, L. M. Flores, F. Campigotto, E. Weller, K. C. Anderson, D. T. Scadden, I. M. Ghobrial, BM mesenchymal stromal cell-derived exosomes facilitate multiple myeloma progression. *J. Clin. Invest.* **123**, 1542–1555 (2013).
23. S. Pece, D. Tosoni, S. Confalonieri, G. Mazzarol, M. Vecchi, S. Ronzoni, L. Bernard, G. Viale, P. G. Pelicci, P. P. Di Fiore, Biological and molecular heterogeneity of breast cancers correlates with their cancer stem cell content. *Cell* **140**, 62–73 (2010).
24. X. H. Zhang, Q. Wang, W. Gerald, C. A. Hudis, L. Norton, M. Smid, J. A. Foekens, J. Massagué, Latent bone metastasis in breast cancer tied to Src-dependent survival signals. *Cancer Cell* **16**, 67–78 (2009).
25. J. A. Aguirre-Ghiso, Models, mechanisms and clinical evidence for cancer dormancy. *Nat. Rev. Cancer* **7**, 834–846 (2007).
26. J. Geng, H. Luo, Y. Pu, Z. Zhou, X. Wu, W. Xu, Z. Yang, Methylation mediated silencing of miR-23b expression and its role in glioma stem cells. *Neurosci. Lett.* **528**, 185–189 (2012).
27. J. C. Loftus, J. T. Ross, K. M. Paquette, V. M. Paulino, S. Nasser, Z. Yang, J. Kloss, S. Kim, M. E. Berens, N. L. Tran, miRNA expression profiling in migrating glioblastoma

cells: Regulation of cell migration and invasion by miR-23b via targeting of Pyk2. *PLOS One* **7**, e39818 (2012).
28. K. Rombouts, V. Carloni, T. Mello, S. Omenetti, S. Galastri, S. Madiai, A. Galli, M. Pinzani, Myristoylated Alanine-Rich protein Kinase C Substrate (MARCKS) expression modulates the metastatic phenotype in human and murine colon carcinoma in vitro and in vivo. *Cancer Lett.* **333**, 244–252 (2013).
29. J. A. Joyce, J. W. Pollard, Microenvironmental regulation of metastasis. *Nat. Rev. Cancer* **9**, 239–252 (2009).
30. C. M. Ghajar, H. Peinado, H. Mori, I. R. Matei, K. J. Evason, H. Brazier, D. Almeida, A. Koller, K. A. Hajjar, D. Y. Stainier, E. I. Chen, D. Lyden, M. J. Bissell, The perivascular niche regulates breast tumour dormancy. *Nat. Cell Biol.* **15**, 807–817 (2013).
31. A. Louissaint Jr., S. Rao, C. Leventhal, S. A. Goldman, Coordinated interaction of neurogenesis and angiogenesis in the adult songbird brain. *Neuron* **34**, 945–960 (2002).
32. I. Malanchi, A. Santamaria-Martínez, E. Susanto, H. Peng, H. A. Lehr, J. F. Delaloye, J. Huelsken, Interactions between cancer stem cells and their niche govern metastatic colonization. *Nature* **481**, 85–89 (2011).
33. M. Al-Hajj, M. S. Wicha, A. Benito-Hernandez, S. J. Morrison, M. F. Clarke, Prospective identification of tumorigenic breast cancer cells. *Proc. Natl. Acad. Sci. U.S.A.* **100**, 3983–3988 (2003).
34. P. S. Mitchell, R. K. Parkin, E. M. Kroh, B. R. Fritz, S. K. Wyman, E. L. Pogosova-Agadjanyan, A. Peterson, J. Noteboom, K. C. O'Briant, A. Allen, D. W. Lin, N. Urban, C. W. Drescher, B. S. Knudsen, D. L. Stirewalt, R. Gentleman, R. L. Vessella, P. S. Nelson, D. B. Martin, M. Tewari, Circulating microRNAs as stable blood-based markers for cancer detection. *Proc. Natl. Acad. Sci. U.S.A.* **105**, 10513–10518 (2008).

Acknowledgments: We thank N. Kai and I. Konishi (Terabase Inc.) for providing electron microscopy images, and S. Miura, C. Kina, and C. Onuma (National Cancer Center Hospital) and A. Inoue (National Cancer Center Research Institute) for excellent technical support. **Author contributions:** M.O., N.K., and T.O. designed the experiments and wrote the manuscript. M.O., N.K., N.T., Y.Y., F.T., and R.T. performed the experiments. M.Y. and H.T. provided the clinical samples. M.O. and K.T. performed the statistical analysis. **Funding:** This work was supported in part by the Grant-in-Aid for the Third-Term Comprehensive 10-Year Strategy for Cancer Control from the Ministry of Health, Labor, and Welfare, Japan; the Program for Promotion of Fundamental Studies in Health Sciences of the National Institute of Biomedical Innovation; and the Japan Society for the Promotion of Science through the Funding Program for World-Leading Innovative R&D on Science and Technology (FIRST Program) initiated by the Council for Science and Technology Policy. **Competing interests:** The authors declare that they have no competing interests. **Data and materials availability:** The gene expression microarray data are deposited in GEO (http://www.ncbi.nlm.nih.gov/geo/), accession numbers GSE57921 and GSE58027.

Submitted 28 February 2014
Accepted 12 June 2014
Final Publication 1 July 2014
10.1126/scisignal.2005231
Citation: M. Ono, N. Kosaka, N. Tominaga, Y. Yoshioka, F. Takeshita, R.-u Takahashi, M. Yoshida, H. Tsuda, K. Tamura, T. Ochiya, Exosomes from bone marrow mesenchymal stem cells contain a microRNA that promotes dormancy in metastatic breast cancer cells. *Sci. Signal.* **7**, ra63 (2014).

Science Signaling
AAAS

Exosomes from bone marrow mesenchymal stem cells contain a microRNA that promotes dormancy in metastatic breast cancer cells

Makiko Ono, Nobuyoshi Kosaka, Naoomi Tominaga, Yusuke Yoshioka, Fumitaka Takeshita, Ryou-u Takahashi, Masayuki Yoshida, Hitoshi Tsuda, Kenji Tamura and Takahiro Ochiya (July 1, 2014)

Science Signaling 7 (332), ra63. [doi: 10.1126/scisignal.2005231]

Science Signaling (ISSN 1937-9145) is published weekly, except the last December, by the American Association for the Advancement of Science, 1200 New York Avenue, NW, Washington, DC 20005.

Annals of Oncology 25: 1973–1979, 2014
doi:10.1093/annonc/mdu247
Published online 9 July 2014

Activated PI3K/AKT and MAPK pathways are potential good prognostic markers in node-positive, triple-negative breast cancer

K. Hashimoto[1], H. Tsuda[2], F. Koizumi[3], C. Shimizu[1], K. Yonemori[1], M. Ando[1], M. Kodaira[1], M. Yunokawa[1], Y. Fujiwara[1] & K. Tamura[1]*

Departments of [1]Breast and Medical Oncology; [2]Pathology and Clinical Laboratories; [3]Shien-laboratory, National Cancer Center Hospital, Tokyo, Japan

Received 10 July 2012; revised 7 September 2013 and 10 June 2014; accepted 16 June 2014

Background: Triple-negative breast cancer (TNBC) patients are a poor prognostic subgroup, and currently, there is no biomarker for targeted therapy.

Patients and methods: Tissue samples were obtained from 75 TNBC patients with lymph-node metastases who had received adjuvant chemotherapy. We examined 11 biomarkers, including *PIK3CA* and *AKT1*mutation, with regard to event-free survival (EFS) and overall survival (OS) of patients.

Results: In the tumor tissues, phospho-AKT (pAKT) expression was significantly related to HER4 expression. Expression of each of these biomarkers was significantly related to longer EFS ($P = 0.024$ and 0.03, respectively). pERK expression was also a good prognostic factor regarding EFS and OS in TNBC ($P = 0.002$ and 0.006, respectively). We also identified a correlation between epidermal growth factor receptor positivity and insulin-like growth factor receptor type 1 positivity ($P = 0.001$). pERK and T-stage (1–3 versus >3) were independent good prognostic factors by multivariate analysis.

Conclusions: We determined that tumors expressing pAKT or pERK are a good prognostic subtype in node-positive TNBC. Different targeted therapies may be necessary for TNBC that involves activation of PI3K/AKT or MAPK pathways.

Key words: biomarkers, MAPK, HER4:PI3K, prognosis, triple-negative breast cancer

introduction

Triple-negative breast cancers (TNBC) are defined as those tumors that lack expression of genes for estrogen receptor (ER), progesterone receptor (PgR), and human epidermal growth factor receptor type 2 (HER2). The majority of TNBCs also have a basal phenotype, which has previously been defined by microarray gene-expression studies [1]. TNBC with expression of cytokeratin 5/6 (CK5/6) and/or HER1 (epidermal growth factor receptor; EGFR), according to immunohistochemistry (IHC), are now considered to have a surrogate basal-phenotype, as defined by microarray [2]. However, as TNBC is heterogeneous, a basal marker alone is insufficient for understanding its tumor biology.

As TNBC is unlikely to benefit from existing targeted therapies, such as endocrine therapy and trastuzumab, conventional chemotherapies are used for its treatment. However, the sensitivity of TNBC to chemotherapy varies, with ~30% of these breast cancer patients achieving complete pathological response with neoadjuvant chemotherapy [3].

Approximately 20% of breast cancers harbor *PIK3CA* mutation, which permits cell growth independent to epidermal growth factors. Thus, it has been hypothesized that *PIK3CA* may have a role in cell survival in TNBC, but its impact on the prognosis of breast cancer patients is controversial [4, 5]. Functional loss of the phosphatase and tensin homolog (PTEN), which is known as a negative regulator of the phosphoinositide 3-kinase (PI3K) signaling pathway, may play a role in activating the PI3K/AKT pathway [6]. The frequency of *AKT1* mutation (E17K) in breast cancer is reportedly 8%, which has been shown to lead to higher kinase activity than that of wild-type *AKT1* [7]. Therefore, AKT integrates various upstream inputs and triggers downstream network activities [8]. The mitogen-activated protein kinase (MAPK)–MAPK kinase (MEK)–extracellular signal-regulated kinase (ERK) cascade also has a fundamental function in the regulation of cell proliferation and survival. Aberrant functioning of MAPK is related to tumorigenesis, and crosstalk between the PI3K/AKT and MAPK pathways has been implicated. ERK1 and ERK2 (ERK1/2) exist downstream of

*Correspondence to: Dr Kenji Tamura, Department of Breast Oncology and Medical Oncology, National Cancer Center Hospital, 5-1-1 Tsukiji, Chuo-ku, Tokyo, Japan. Tel: +81-3-3542-2511; Fax: +81-3-3542-3815; E-mail: ketamura@ncc.go.jp

MAPK signaling and integrate various upstream signal transductions [9].

Previous studies have demonstrated that these signal cascades are up-regulated in TNBC [8]. However, the role(s) of these cascades in TNBC and how they are activated by their upstream receptors are unknown. In this study, we used TNBC samples to identify biomarkers that up-regulate PI3K/AKT or MAPK pathways in relation to patients' clinical outcomes.

patients and methods

patients

Patients included in this analysis had to meet the following criteria: breast cancer patients who underwent lumpectomy or mastectomy between 2002 and 2008 at the National Cancer Center Hospital; who received at least one regimen of adjuvant chemotherapy following breast surgery; who were pathologically identified to have at least one axillary lymph-node metastasis; who had no history of previous chemotherapy or endocrine therapy; and diagnosed with TNBC. TNBC was defined as ER-negative, PgR-negative, and HER2-negative [10, 11].

immunohistochemistry and polymerase chain reaction

We used both primary FFPE tumor samples and methanol-fixed paraffin-embedded metastatic lymph-node samples for gene mutation analysis. For IHC, 4-μm-thick sections of whole tissue were deparaffinized in xylene and rehydrated in ethanol. All sections were incubated in 3% hydrogen peroxidase in 100% methanol for 30 min to remove endogenous peroxidase activity. All antibodies information and IHC conditions are listed in supplementary Table S1, available at *Annals of Oncology* online. A substrate–chromogen mix was used for visualization of the immunoreactions. Meyer's sour hematoxylin was used as the counter stain. Evaluation of IHC was performed by two authors (KH and HT) who were initially blind to the clinical information.

Table 1. Patient characteristics ($n = 75$)

Gender	Female	75
Age, median, range		56 (28–82)
Histopathology	Invasive ductal carcinoma	62
	Invasive lobular carcinoma	3
	Aprocrine carcinoma	8
	Others	2
T-stage	T1	22
	T2	37
	T3	15
	T4	1
Number of lymph-node metastases	1–3	45
	≥4	30
Surgery	Mastectomy	49
	Lumpectomy	26
Tumor grade	Grade 1–2	17
	Grade 3	58
Adjuvant chemotherapy	Anthracyclines and taxanes	45
	Anthracyclines only	20
	Taxanes only	7
	Fluorouracil	3

Table 2. Expression or mutation of each biomarker

Markers	Number ($n = 75$)	%
PIK3CA mutation	26	35
H1047R	15	
E545K	11	
None	49	
Akt1 mutation		
E17K	0	0
None	45	
Not applicable	30	
PTEN		
Loss	40	53
Expression	35	
HER1		
Over-expression	44	59
Low/null	31	
HER3		
Expression	47	63
Low/null	28	
HER4 (membrane)		
Expression	31	41
Low/null	44	
HER4 (cytoplasmic)		
Expression	46	61.3
Low/null	29	
HER4 (nucleus)		
Expression	10	13.3
Low/null	65	
pHER4 (cytoplasmic)		
Expression	66	88
Low/null	9	
pHER4 (nucleus)		
Expression	24	32
Low/null	51	
IGF1R		
Over-expression	45	60
Low/null	30	
pAKT		
Expression	40	53
Null	35	
pERK		
Expression	29	39
Null	46	
CK5/6		
Expression	39	52
Low/null	36	
Subtypes		
Basal	53	71
Non-basal	22	
ALDH1		
Expression	49	65
Low/null	26	

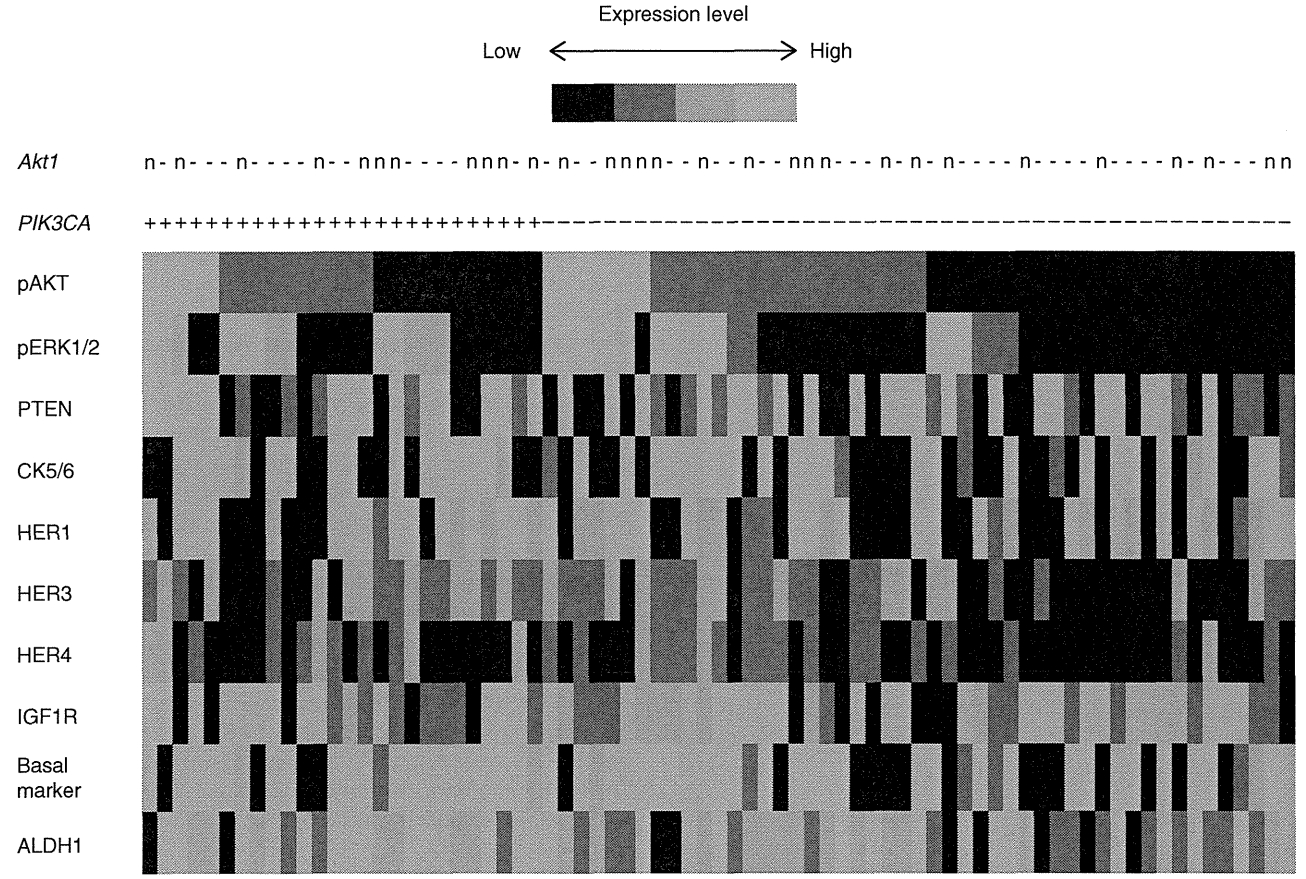

Figure 1. Mapping of protein expression determined by immunohistochemistry and a gene mutation assay of *PIK3CA* and *AKT1*. The expression level was indicated by green (null), yellow (low), pink (middle), and high (red). An 'n' in the row labeled *AKT1* indicates that the results of amplification and sequencing of DNA were unavailable. The basal marker included a higher expression level of either cytokeratin 5 and 6 (CK5/6) or human epidermal growth factor receptor (HER) 1.

For evaluation of phospho-AKT (pAKT), phospho-ERK (pERK), and PTEN, presentation of >10% of positive cancer cells was considered positive for each marker, and tumors were graded according to the staining intensity, where 0, no staining; 1, light staining; 2, moderate staining; and 3, strong staining (supplementary Figures S2 and S3, available at *Annals of Oncology* online). For HER1, HER3, and insulin-like growth factor receptor-1 (IGF1R), we applied the evaluation methods used previously for HER2 [11]. For HER4, both membrane, cytoplasmic, and nuclear immunoreactivity were evaluated. Phosphorylated HER4 was also evaluated by two different antibodies (pTyrY1162 and pTyrY1188) in cytoplasm and in nuclei (supplementary Figures S4 and S5, available at *Annals of Oncology* online). For evaluation of CK5/6 and aldehyde dehydrogenase 1 (ALDH1), the presence of >5% positive cancer cells was considered positive for each marker.

Genomic DNA was extracted after macro-dissection of tissues, using hematoxylin–eosin stain as a reference marker. *PIK3CA* gene mutations in exon 9 (E542K, E545K/D) or exon 20 (H1047R) were detected with an ARMS/Scorpions primer PI3K mutation test kit (PK01; QIAGEN, Tokyo, Japan) [12]. For *AKT1* mutation analysis, we designed the following primer pair to detect E17K mutation: forward primer, 5′-ATCCCAGGCACATC TGTCCT-3′, and reverse primer, 5′-TAGGACTCAGCCTGGAGACT-3′.

statistical analysis

Detection of the associations of each biomarker examined in this analysis was carried out using the χ^2 tests. Event-free survival (EFS) was defined as the time from surgery until the detection of recurrence or death due to any cause. The overall survival (OS) was defined as the time from surgery until the date of death or the most recent follow-up. The median EFS and median survival time (MST) were calculated using the Kaplan–Meier method, and significance was determined using the log-rank test. The significant differences between variables were determined with two-sided *t*-tests, and these calculations were carried out with SPSS, version 19 (IBM, Okinawa, Japan).

results

patient characteristics and biomarkers

We identified 75 TNBC patients who met the eligibility criteria. The characteristics of these patients are listed in Table 1. Anthracycline-containing regimens included doxorubicin and cyclophosphamide or epirubicin, fluorouracil, and cyclophosphamide. Taxane-containing regimens included paclitaxel or docetaxel.

gene mutation assay and immunohistochemical study

Table 2 shows the frequency of expression or mutation of each biomarker. We found that 26 tumors (35%) harbored *PIK3CA* mutations, of which 15 were of H1047R and 11 were of E545K.

Table 3. Related factors with phosphorylation of AKT or ERK1/2

	P-value
AKT phosphorylation	
PIK3CA mutation	0.63
HER1	0.64
HER3	0.23
HER4 (membrane)	0.004
HER4 (cytoplasmic)	0.001
HER4 (nucleus)	>0.9
pHER4 (cytoplasm)	0.04
pHER4 (nucleus)	>0.9
IGF1R	0.17
PTEN	0.64
ALDH1	0.23
Basal subtype	0.62
pERK	0.10
ERK1/2 phosphorylation	
PIK3CA mutation	0.21
HER1	0.64
HER3	0.09
HER4 (membrane)	0.35
HER4 (cytoplasmic)	0.28
HER4 (nucleus)	0.73
pHER4 (cytoplasm)	0.01
pHER4 (nucleus)	0.62
IGF1R	0.17
PTEN	0.25
ALDH1	1.00
Basal subtype	0.44

In contrast, no *AKT1* mutations were detected in 45 samples that were successfully sequenced. Expression of each marker in accordance with *PIK3CA* and *AKT1* mutations are shown in Figure 1.

Subsequently, we examined which factors may contribute to activation of the PI3K/AKT or MAPK pathways. We found that pAKT was related to HER4 expression (membrane, $P = 0.004$; cytoplasmic, $P = 0.001$) and phosphorylated HER4 in cytoplasm ($P = 0.04$) (Table 3). pERK was related to cytoplasmic pHER4 expression ($P = 0.01$). Among the correlations examined, HER1 and IGF1R ($P = 0.001$) were significantly related to each other.

survival analysis

We analyzed pAKT and pERK in relation to EFS and OS in a median follow-up period of 63.2 months. The median EFS of those patients with pAKT positivity or negativity was not reached until or 79.4 months, respectively ($P = 0.024$) (Figure 2A). For OS, we did not detect a significant difference between the pAKT groups. Furthermore, the tumors that were pAKT-positive or -negative were not statistically different in terms of the number of lymph-node metastases (1–3 versus ≥4), T-stage (T1–2 versus T3–4), tumor grade (grade 1–2 versus 3), or chemotherapy regimens (anthracycline followed by taxanes versus others). Because HER4 and pAKT were significantly correlated with each other (Table 3), we then assessed HER4 expression with regard to EFS and OS. The median EFS for patients with HER4-positive tumors was significantly longer than that for patients with HER4-negative tumors (membrane: not reached versus 79.4 months, $P = 0.03$; cytoplasmic: not reached versus 89.7 months, $P = 0.04$, nuclear: not reached versus 86.2 months, $P = 0.03$) (Figure 2B). Phosphorylated HER4 was prone to good prognosis in EFS, although statistical significance was not identified (cytoplasmic: $P = 0.077$, nuclear: $P = 0.279$). Regarding OS, both HER4 and pHER4 expressions were not a factor for survival. The tumors that were HER4-positive or -negative were statistically different in terms of the number of lymph-node metastases [number of metastases in HER4-positive tumors, 1–3 (77%) versus ≥4 (23%), $P = 0.02$], but not in terms of T-stage, tumor grade, and chemotherapy regimens.

We also found that both EFS and OS were significantly longer for patients with pERK-positive tumors than for those with pERK-negative tumors (median EFS; not reached versus 62.2 months, $P = 0.002$, MST; not reached versus not reached, $P = 0.006$, respectively) (Figure 2C and D). However, no differences were found in pERK-positive versus -negative tumors in terms of the following criteria: number of lymph-node metastases, T-stage, tumor grade, or chemotherapy regimen. *PIK3CA* mutation status was not correlated with EFS and OS, although this was associated with basal marker.

In univariate analysis for EFS, T-stage (3 versus others), number of lymph node (>3 versus 1–3), pAKT, pERK, and pHER4 (cytoplasmic) were statistically significant good prognostic marker (Table 4). In multivariate analysis, pERK and T-stage (1–3 versus >3) remained as good prognostic marker.

discussion

In this biomarker analysis aimed to explore potential therapeutic targets of TNBC, we determined both that HER4 expression is associated with phosphorylated AKT expression, and that tumors expressing either HER4 or pAKT were associated with patients with better prognosis. Furthermore, tumors that expressed phosphorylated ERK were also associated with better prognosis than tumors lacking pERK.

HER4 has been reported as a good prognostic marker in breast cancers not limited to the triple-negative subtype. Witton et al. [13] reported that HER4 is the only good prognostic marker, whereas other HER family members are negatively related to survival, possibly because HER4 is related to ER positivity and low tumor grade. Of note, we examined the HER4 expression pattern in both the membrane, the cytoplasm, and nuclear, because the intracellular domain of HER4 has been reported as a good prognostic factor [14, 15]. For phosphorylated HER4 (pHER4), we used two different antibodies (pTyrY1162 and pTyrY1188) (supplementary Figures S4 and S5, available at *Annals of Oncology* online). We confirmed the specificity of these antibodies by abolition of staining following pre-incubation of them with the phospho peptide (0.1 mg/ml, Abnova) (Supplementary Figure S6, available at *Annals of Oncology* online). HER4 expressions were detected both in membrane, in cytoplasm, and in nuclei. In contrast, pHER4 expressions were detected in cytoplasm and nuclei, but not in membrane. HER4 levels in all subcellular localization were associated with good prognosis in EFS. Cytoplasmic and nuclear pHER4 levels were prone to good prognosis but not statistically

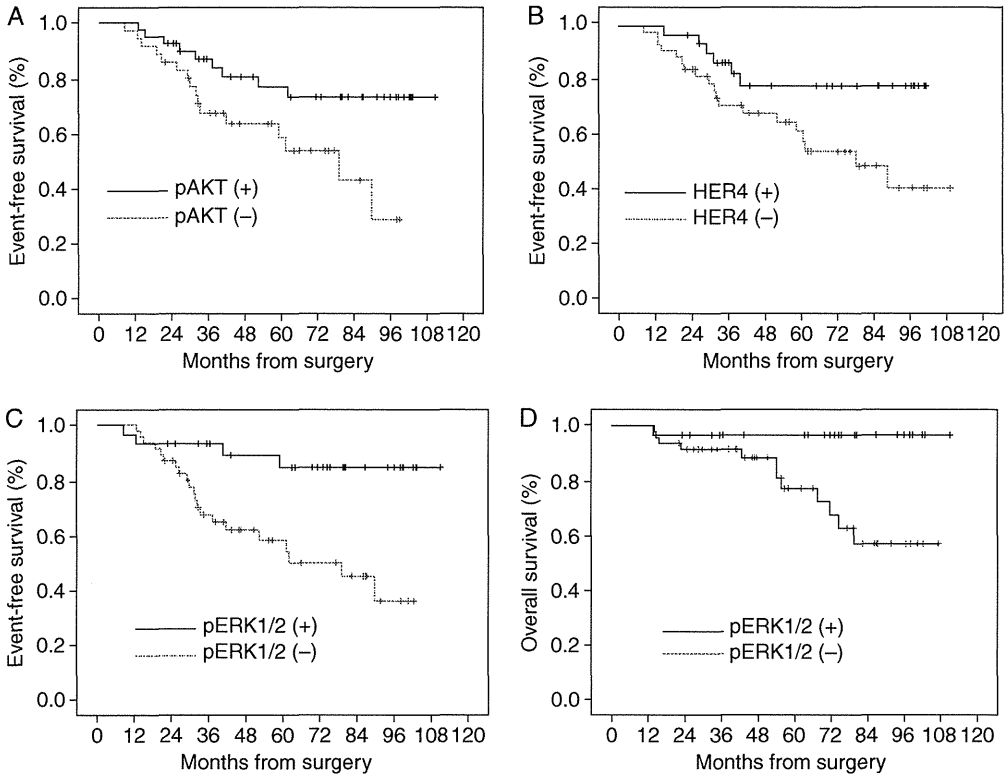

Figure 2. Survival curves obtained with the Kaplan–Meier method. (A) Event-free survival curve with expression of phospho-AKT [pAKT (+); green line] or no pAKT [pAKT (−); blue line]. (B) Event-free survival curve with expression of human epidermal growth factor receptor 4 [HER4 (+); green line] or no HER4 expression [HER4 (−); blue line]. (C) Event-free survival curve with expression of phospho-ERK 1 and 2 [pERK1/2 (+); green line] or no expression of pERK1/2 [pERK1/2 (−); blue line]. (D) Overall survival curve with expression of pERK1/2 (+), green line, or no expression of pERK1/2 [pERK1/2 (−); blue line].

significant (supplementary Figure S7, available at *Annals of Oncology* online). HER4 may play a role in the process that leads to apoptosis or decreased activity of cell proliferation, such that tumors that express HER4 may be associated with a good prognosis [15].

Previously, some studies have reported activation of the PI3K/AKT or MAPK pathways as a negative prognostic factor, whereas others have reported that these factors did not relate to survival [16]. Furthermore, ALDH-1, a potential stem cell marker in breast cancer, has also been reported as a negative prognostic marker in breast cancer, whereas IGF1R expression and *PIK3CA* mutation are reportedly related to better clinical outcomes [4, 17–19]. Regarding the MAPK pathway, there was a previous report that the expression level of MAPK was related to chemosensitivity in hormone receptor-negative tumors [20]. In contrast, other reports have suggested that activation of the MAPK pathway is associated with chemoresistance [16]. These discrepant results from previous reports may be due to the selection of the breast cancer cohorts. In this study, we limited enrollment to unique TNBC patients who had lymph-node metastases, whereas some other studies have included skewed breast cancer subtypes. Thus, the possibility remains that previous results may reflect the outcomes of poor-prognosis subgroups, including triple-negative or HER2-subtypes, as these markers seem highly related to triple-negative or HER2-subtypes rather than to hormone receptor-positive subtypes [18, 21]. In this study, PIK3CA mutation status was not correlated with survival, although this was associated with basal marker positive which was already reported to be chemo-sensitive. Phosphorylated Akt would be affected not only by PI3CA mutation but also by AKT1 mutation, PTEN loss, or MAGI3-Akt3 fusion gene. The discrepancies with prognosis from the previous reports might be influenced chemosensitivities which are related with pERK, PI3CA, or AKT1 mutation status, because all presented patients have received adjuvant chemotherapies.

Interpretation of the present results should be done cautiously because this study has some limitations. First, patients included in this analysis were pathologically identified as having lymph-node-positive TNBCs. Generally, the primary tumor size and the number of lymph-node metastases are significant prognostic factors in breast cancer. However, in lymph node-positive TNBCs, prognosis may not be affected by the number of lymph-node metastases. Secondly, chemotherapy containing anthracycline followed by taxanes may benefit TNBC patients. To reduce this factor, we carried out the χ^2 tests for each biomarker to identify prognostic factors relevant by the number of lymph-node metastases, tumor size, tumor grade, and chemotherapy regimens.

In summary, we revealed a correlation between HER4 and pAKT expression, and found that both factors were associated

Table 4. Univariate and multivariate analysis for event-free survival

Variables	HR	95% CI	*P*-value
Univariate analysis			
T-stage (3 versus others)	3.34	1.46–7.64	0.008
n. of lymph node (>3 versus 1–3)	3.06	1.37–6.83	0.006
Tumor grade (3 versus others)	2.48	0.74–8.29	0.14
pAKT (+ versus −)	0.4	0.17–0.91	0.03
pERK (+ versus −)	0.22	0.07–0.64	0.01
PI3K mutation (+ versus −)	0.77	0.33–1.78	0.54
PTEN (+ versus −)	1.39	0.63–3.04	0.42
ALDH1 (+ versus −)	0.66	0.30–1.46	0.31
IGF1R (+ versus −)	0.86	0.39–1.9	0.71
HER1 (+ versus −)	1.2	0.54–2.68	0.66
HER3 (+ versus −)	0.78	0.35–1.74	0.55
HER4 (+ versus −)	0.45	0.20–0.99	0.05
pHER4 (Y1188) cytoplasm (+ versus −)	0.56	0.31–0.82	0.08
pHER4 (Y1188) nucleus (+ versus −)	1.8	0.61–5.3	0.28
Multivariate analysis			
pAKT (+ versus −)	0.68	0.25–1.81	0.68
pERK (+ versus −)	0.24	0.08–0.72	0.01
T-stage (3 versus others)	3.91	1.62–9.41	0.002
n. of lymph node (>3 versus 1–3)	2.22	0.98–5.06	0.06
HER4 (+ versus −)	0.53	0.21–1.33	0.18

+, over-expression or high level; −, low expression or null, or low level.

with longer EFS. Furthermore, we determined that pERK expression was also related to longer EFS and OS periods, and was an independent good prognostic factor after multivariate analysis including clinicopathological features as well as T-stage.

acknowledgements

We thank all the study participants who provided tissue samples for this analysis. We also thank Ms. A. Otsuka, Ms. Y. Kitamura from Shien-Laboratory, and Ms. C. Kina and Ms. S. Miura from the Department of Pathology for technical advice. We also thank Ms. N. Nakamura, Ms. M. Akitaya, and Ms. R. Koyama for secretarial support of this study.

funding

This study was funded by a grant from the Third-Term Comprehensive Control Research for Cancer from the Ministry of Health, Labor, and Welfare of Japan (H22-general-23).

disclosure

The authors have declared no conflicts of interest.

references

1. Sorlie T, Tibshirani R, Parker J et al. Repeated observation of breast tumor subtypes in independent gene expression data sets. Proc Natl Acad Sci USA 2003; 100: 8418–8423.
2. Cheang MC, Voduc D, Bajdik C et al. Basal-like breast cancer defined by five biomarkers has superior prognostic value than triple-negative phenotype. Clin Cancer Res 2008; 14: 1368–1376.
3. Carey LA, Dees EC, Sawyer L et al. The triple negative paradox: primary tumor chemosensitivity of breast cancer subtypes. Clin Cancer Res 2007; 13: 2329–2334.
4. Kalinsky K, Jacks LM, Heguy A et al. PIK3CA mutation associates with improved outcome in breast cancer. Clin Cancer Res 2009; 15: 5049–5059.
5. Berns K, Horlings HM, Hennessy BT et al. A functional genetic approach identifies the PI3K pathway as a major determinant of trastuzumab resistance in breast cancer. Cancer Cell 2007; 12: 395–402.
6. Weigelt B, Warne PH, Downward J. PIK3CA mutation, but not PTEN loss of function, determines the sensitivity of breast cancer cells to mTOR inhibitory drugs. Oncogene 2011; 30: 3222–3233.
7. Carpten JD, Faber AL, Horn C et al. A transforming mutation in the pleckstrin homology domain of AKT1 in cancer. Nature 2007; 448: 439–444.
8. Zhao JJ, Liu Z, Wang L et al. The oncogenic properties of mutant p110alpha and p110beta phosphatidylinositol 3-kinases in human mammary epithelial cells. Proc Natl Acad Sci USA 2005; 102: 18443–18448.
9. Sebolt-Leopold JS, Herrera R. Targeting the mitogen-activated protein kinase cascade to treat cancer. Nat Rev Cancer 2004; 4: 937–947.
10. Allred DC, Harvey JM, Berardo M, Clark GM. Prognostic and predictive factors in breast cancer by immunohistochemical analysis. Mod Pathol 1998; 11: 155–168.
11. Wolff AC, Hammond ME, Schwartz JN et al. American Society of Clinical Oncology/College of American Pathologists guideline recommendations for human epidermal growth factor receptor 2 testing in breast cancer. J Clin Oncol 2007; 25: 118–145.
12. Board RE, Thelwell NJ, Ravetto PF et al. Multiplexed assays for detection of mutations in PIK3CA. Clin Chem 2008; 54: 757–760.
13. Witton CJ, Reeves JR, Going JJ et al. Expression of the HER1–4 family of receptor tyrosine kinases in breast cancer. J Pathol 2003; 200: 290–297.